DESIGN AND ANALYSIS OF A NOVEL COMPLIANT CONSTANT FORCE GRIPPER

YENİ BİR SABİT KUVVETLİ ESNEK TUTUCUNUN TASARIMI VE ANALİZİ

İSA ÖMER IŞIKDOĞAN

PROF. DR. ENGİN TANIK

Supervisor

Submitted to

Graduate School of Science and Engineering of Hacettepe University

as a Partial Fulfillment to the Requirements

for the Award of the Degree of Master of Science

in Mechanical Engineering

2020

ÖZET

YENİ BİR SABİT KUVVETLİ ESNEK TUTUCUNUN TASARIMI VE ANALİZİ

İSA ÖMER IŞIKDOĞAN

Yüksek Lisans, Makina Mühendisliği Bölümü

Tez Danışmanı: Prof. Dr. Engin TANIK

Haziran 2020, 68 sayfa

Bu tez çalışmasının amacı yeni bir sabit kuvvetli esnek tutucu tasarlamaktır. Sabit kuvvetin elde edildiği aralığı artırmak ve bu aralıktaki kuvvetin büyüklüğündeki sapmaları azaltmak tezin ana hedefleri arasındadır. Tez modeli iki adet esnek uzun parçadan oluşan kol kızak mekanizması tabanlıdır. Bu mekanizmanın analizi Sahte Rijit Cisim Metodu ve Sanal İş Prensibi kullanılarak yapılacaktır. Modele ait tasarım parametreleri sezgisel olarak optimize edilerek üç boyutlu boyutsuz tasarım şablonları çıkarılmıştır. Bu şablonlar kullanılarak iki farklı uzuv boyut oranı ve katılık katsayısı belirlenmiştir. Belirlenen bu oranlarla oluşturulan model, sonlu elemanlar yazılımı kullanılarak test edilmiş ve teorik yaklaşımla oldukça yakın sonuçlar elde edilmiştir.

Anahtar Kelimeler: Esnek Mekanizma, Sabit Kuvvetli Esnek Mekanizma, Sahte Rijit Cisim Metodu, Sanal İş Prensibi

ABSTRACT

DESIGN AND ANALYSIS OF A NOVEL COMPLIANT CONSTANT FORCE GRIPPER

İsa Ömer IŞIKDOĞAN

Master of Science, Department of Mechanical Engineering

Supervisor: Prof. Dr. Engin TANIK

June 2020, 68 pages

The aim of this study is to introduce a novel compliant mechanism that has constant force characteristics. Maximizing the constant force stroke and minimizing the force fluctuation are the main objectives. The proposed design model is based on a compliant slider-crank mechanism which consists of two long compliant segments connected with a revolute joint. The analysis of mechanism is performed by using Pseudo Rigid Body Method and Virtual Work Method. Design parameters are optimized heuristically and some 3D design charts are introduced. Two specific non-dimensionless link proportions and segment stiffnesses are synthesized. By using a FEA software the mechanism is analyzed numerically as well. The comparison verified that the analytical approach and simulation results are in a close agreement.

Keywords: Compliant Mechanism, Constant Force Mechanism Pseudo Rigid Body Method, Virtual Work Method

ACKNOWLEDGEMENTS

Firstly, I would like to express my profound thankfulness to my respectable supervisor, Prof. Dr. Engin Tanık, for his encouragement, guidance and supervision. I completed this study with the help of him.

Also I would like to thank Asst. Prof. Dr. Çağıl Merve Tanık, Dr. Mehmet Nurullah Balcı, and Dr. Raşit Karakuş for their support.

Finally, I would like to give thanks to my wife for her moral support, patience and endless love.

İsa Ömer IŞIKDOĞAN

June 2020, Ankara

TABLE OF CONTENTS

LIST OF TABLES

LIST OF FIGURES

LIST OF SYMBOLS AND ABBREVIATIONS

PRBM : Pseudo Rigid Body Model

δ : Displacement

γ : Characteristic Radius Factor

K_θ : Stiffness Coefficient

I : Moment of Inertia,

E : Modulus of Elasticity

K : Non-dimensionless Stiffness Ratio

R : Non-dimensionless Link Length Ratio

Ψ : Force Fluctuation Ratio

1. INTRODUCTION

Mechanisms are basic parts of machines, which can transfer motion, force, and energy from the input to the output, generally by the relative motion of its links. Conventionally relative motion is provided by rigid joints like revolute and sliding joints [1] .

In the recent years, compliant mechanisms have been in progress because of its advantages like low cost, reduced part count, no or less backlash, light weight, and ease in miniaturization which will be detailed in the upcoming sections. Compliant mechanisms are different from rigid mechanisms by the way they acquire relative link motion. Partially compliant mechanisms achieve relative motion not only by the rigid joints but also from deflection of flexible links. Fully compliant mechanisms do not have classical rigid joints in their structure. Also compliant mechanisms can store energy in the form of strain energy which makes them very suitable for special purpose mechanisms like constant force mechanisms and bistable mechanisms [2].

In Figure 1.1-a, a conventional slider crank mechanism is presented where there are three revolute joints and one sliding joint. Rigid slider crank mechanisms have various compliant equivalents. In Figure 1.1-b, a partially compliant slider crank mechanism with a small length flexural pivot is presented. Instead of a rigid joint between coupler and slider, rotation of the coupler link is provided by the deflection of a small length flexural pivot [3].

(a) (b)

Figure 1.1 (a) Rigid Slider Crank Mechanism – (b) Compliant slider crank mechanism [3]

1.1. Aim and Scope of the Study

Constant force mechanisms are in progress in recent years where precision manipulation is important. Conventionally, in machines and robotic devices, constant force is obtained by sensors (Figure 1.2), complex algorithms which yields high cost and low reliability. Instead of this expensive system, compliant constant force mechanisms become popular nowadays. Approximate constant force characteristics can be achieved by compliant constant force mechanisms mechanically which eliminates sensors and algorithms [4].

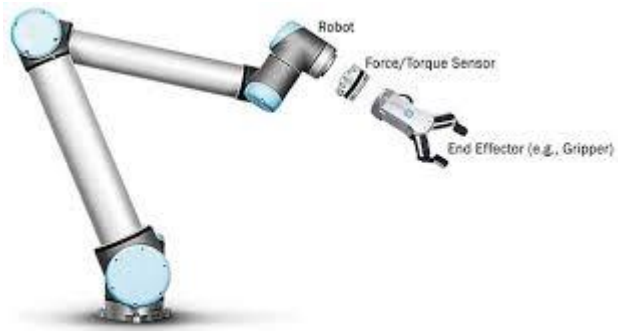

Figure 1.2 Gripper with force sensor

The aim of this study is to develop a compliant mechanism that performs constant force for a large stroke. Generally, it is impossible to obtain exact constant force for the whole stroke. According to the design, constant force can be achieved for some percentage of the total displacement. Briefly, maximizing constant force range and minimizing force fluctuation are valuable properties.

1.2. Advantages of Compliant Mechanisms

Compliant mechanisms have some advantages and disadvantages compared to the rigid body counterparts. First, the details of advantages of compliant mechanism are discussed.

Fewer numbers of parts can be used to carry out a prescribed duty by using compliant mechanisms. The compliant over-running clutch is a good example for the part count reduction. The complaint version (Figure 1.3-a) is produced as one piece and its rigid body equivalent (Figure 1.3-b) which does the same work has components more than ten. The decrease in the number of components can save from assembly time and manufacturing cost.

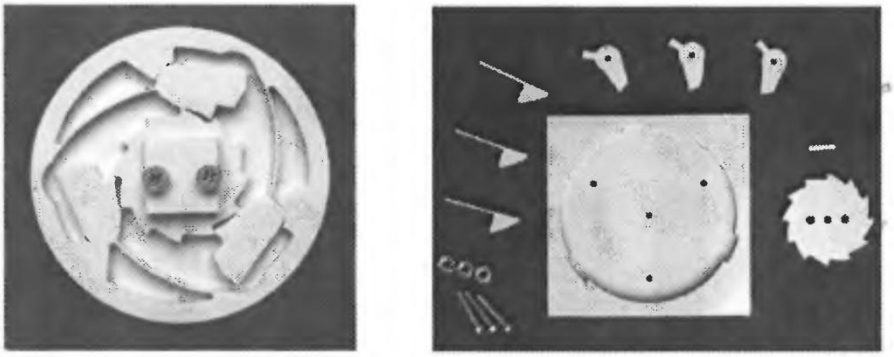

Figure 1.3 (a) Compliant over-running clutch - (b) Its rigid body equivalent [5]

Complaint mechanisms may be fully or partially according to the main classification criteria. If one of the conventional rigid kinematic pairs such as revolute, sliding etc. is involved in the mechanism, the mechanism is called as partially compliant. If all motion is caused by deflection of links, mechanism is called fully compliant. Fully compliant mechanisms do not possess revolute or sliding joints in their structure, so the need for lubrication, maintenance, and wear risks decrease. As seen in Figure 1.4 the compliant crimping mechanism does not have any traditional joints, thus the motion is based upon the elastic deformation of the compliant segments. If it does not possess deflecting ability, it will be a structure and thus will be immobile.

Figure 1.4 Compliant crimping device [5]

For the cases where a mechanism is hard to access or operates in rough conditions which affect the pairs negatively, compliant mechanisms are invaluable for these types of environments. A compliant gripping mechanism (Figure 1.5) is a good example for mechanisms for operating in adverse environments. This mechanism can hold computer

chips while waiting in the chemicals during the manufacturing process. When compliant links are in deflected position, energy is kept as strain energy so the spring effect can easily be included. Thus there is no need for external force or springs to hold the link. Once the link is kept stationary, the deflected beam can preserve the position.

Figure 1.5 Compliant die gripper [2]

When number of joints is decreased, a mechanism can have higher precision. Conventional rigid joints generally have clearance or backlash. For the cases where, number of joints increase, cumulative error of clearances increase and create a significant backlash. Reducing clearances and backlash may dramatically increase the cost [6] for the conventional mechanisms . Due to the nature of compliant mechanisms having fewer or no kinematic pairs cause a reduction in backlash. This property makes compliant mechanisms very appropriate for higher precision measurement devices such as seen in Figure 1.6.

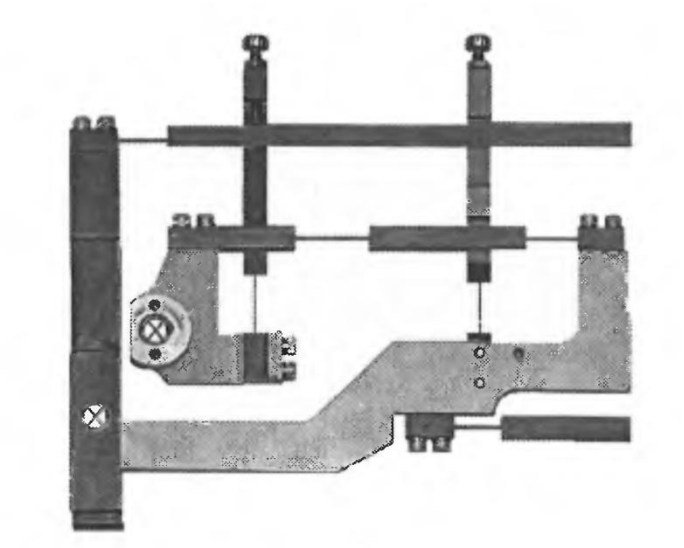

Figure 1.6 High precision compliant mechanism [7]

There are numerous compliant mechanisms materials available in the industry. Among them, one of the most important one is polypropylene which is a thermoplastic. The average density of the polypropylene is around 950 kg/m^3 which is approximately eight times lower than steel. Therefore, significant weight reduction can be achieved with this material. Also polypropylene has the ratio of yield strength to modulus of elasticity ($\frac{S_y}{E}$) equal to 25 which is very high value. This ratio specifies how much a beam can go into a larger deflection without failure which is very important in designing compliant mechanisms.

1.3. Disadvantages of Compliant Mechanisms

Besides the numerous favorable properties, compliant mechanisms are disadvantageous for some applications. The most important challenge is the difficulty of analysis and design of compliant mechanisms because of the large non-linear deflections which denies to use the small deflection beam equations.

As mentioned before, energy storage in the deflected flexible bodies may be used to replace springs and this storage capability is helpful in designing special type constant force mechanisms and bistable mechanisms. However, if the aim of the mechanism is to transfer energy, energy storage ability becomes an energy consuming adverse property.

In conventional rigid mechanisms, links rotate or slide relatively by the help of kinematic pairs, but in compliant mechanisms deflection is a requirement for movability. Even for

fully compliant mechanisms all of the motion is obtained from deflection of the flexible joints. Thus, fatique issue becomes an important because of the cyclic loads applied on flexible beams during the motion of mechanism.

Creep which is the deformation with time under a load even below the yield strength is critic for thermoplastic materials. For steel creep occurs at high temperatures whereas for polymers may have the creep issue at room temperatures. Also stress relaxation may occur when a compliant member is hold under stress.

2. CONSTANT FORCE

For a specific range of displacement, constant force mechanisms apply force with a minor fluctuation. Constant force mechanisms are used in grippers that holds fragile objects of varying sizes, eye surgery robots, robot arm end effectors working on changing part tolerances such as painting, glass cutting.

In Figure 2.1 an ideal case for a constant force mechanism is presented in which the output force never changes for the whole range of motion.

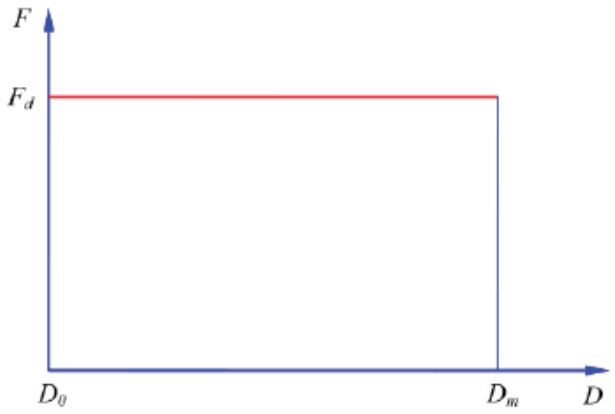

Figure 2.1 Force vs Displacement for the ideal constant force case

The reaction force of an initially stress free compliant member is zero when no load is applied on it. Generally, for constant force compliant mechanisms, constant force cannot be obtained at the beginning of the stroke. A transition zone is required to reach the desired force magnitude as in Figure 2.2. While optimizing a constant force mechanism, keeping this transition zone as small as possible is a valuable property.

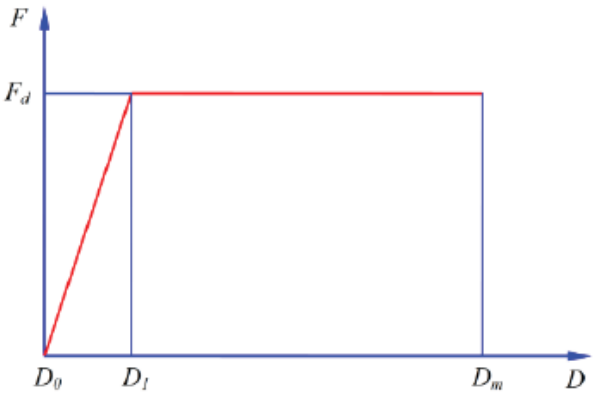

Figure 2.2 Force vs displacement with a transition zone

The sharp edges at the force displacement graph are not expected due to the nature of mechanisms. Generally, mechanisms perform smoother behavior during their working strokes. Thus, smooth curves with a fluctuation are the most common case of such constant force mechanisms (Figure 2.3). At design stage, minimizing the force fluctuation and increasing range of constant force are the main objectives.

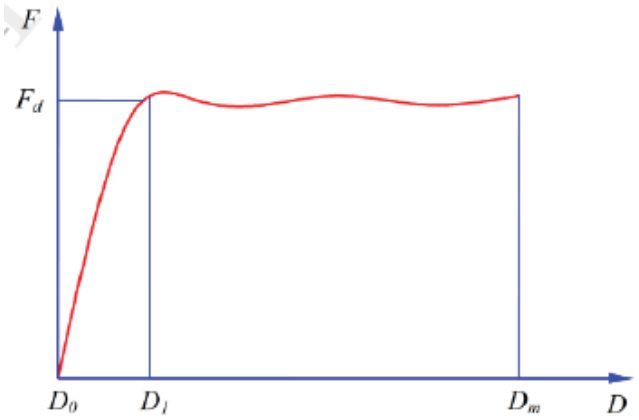

Figure 2.3 Typical force vs displacement graph for a constant force gripper

2.1. Literature Survey

2.1.1. Conventional Constant Force Mechanisms

Nahar and Sugar [8] designed an orthogonally placed double slider mechanism (Figure 2.4). The sliders are connected with a rigid link by revolute pairs and two coil springs are in compression when the external force is applied. If both of the spring stiffnesses are the same, the output force depends on the rigid link length and the spring stiffness. Manufacturing this type of mechanism and the mathematical model is simple; however friction and backlash yield some error from the expected constant force target.

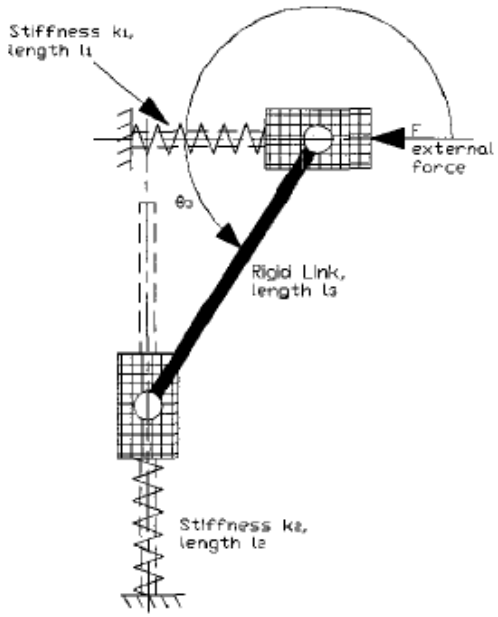

Figure 2.4 Double Slider Mechanism [8]

Nathan [9] proposed a hinged lever (Figure 2.5) constant force mechanism that consists of a lever with a revolute joint and coil spring. The mathematical model is simple and output force is dependent on k_1, l_1, l_2, l_3 and the mechanism can easily be designed to the needed criteria however friction may decrease the performance. A surgical laser is a typical sample for this type of mechanism (Figure 2.6).

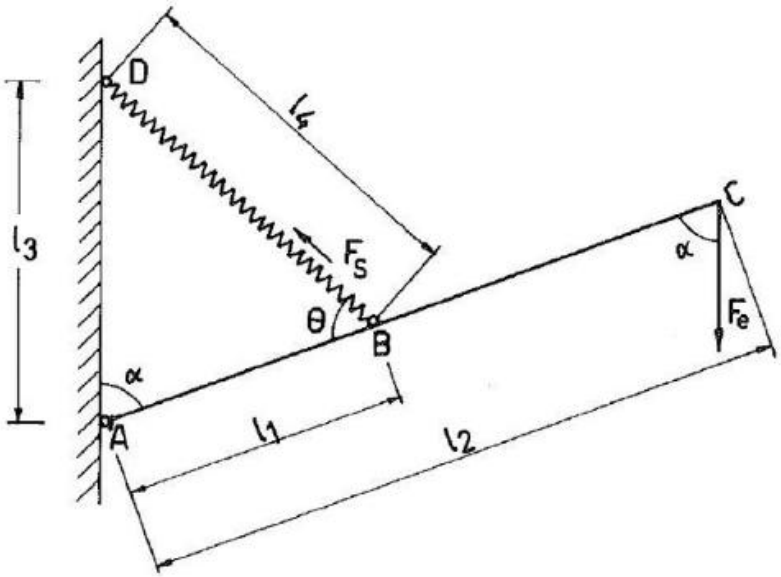

Figure 2.5 Hinged lever mechanism

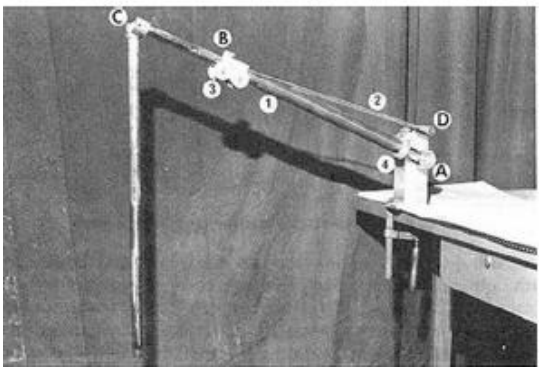

Figure 2.6 Surgical laser

Carella et all [10] worked on oblique spring constant force mechanism (Figure 2.7) in which two of the springs were inclined with the horizontal axis and the other one is vertically placed. During the downward motion of point *P*, the vertical spring is in compression and behaves in positive stiffness manner. The angled springs are compressed initially and then released. While releasing, the springs act in negative stiffness behavior. If stiffnesses of the springs attentively designed, zero stiffness can be acquired. This type of mechanisms are used in vibration isolation.

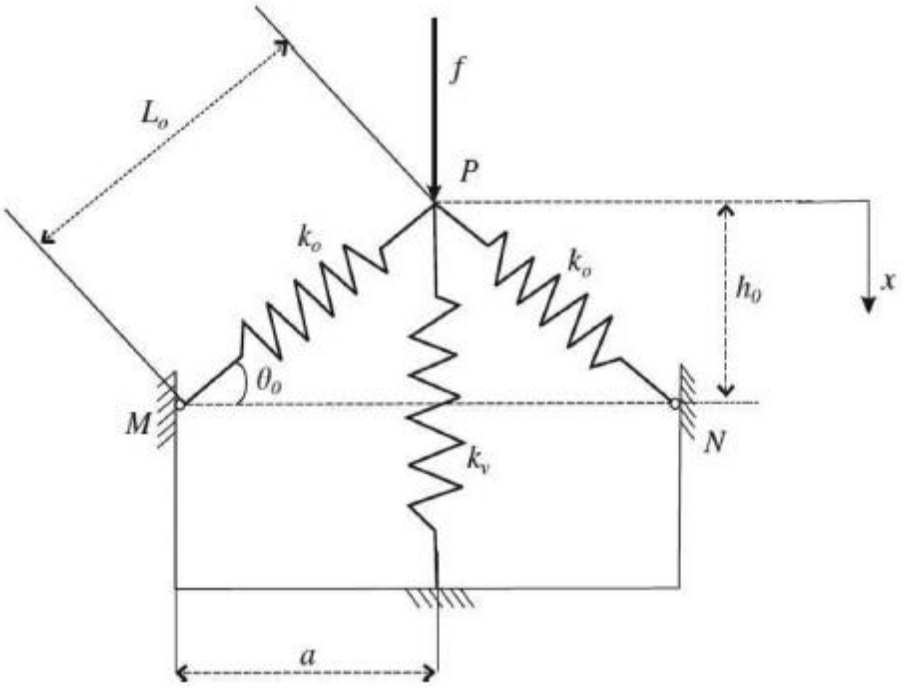

Figure 2.7 Oblique spring mechanism [10]

Liu et all [11] developed a curved surface constant force mechanism (Figure 2.8) . While the curved surface moves in negative y-direction, two sliders with coil springs exert a normal force on it. During this motion, horizontal displacement of sliders in the x-direction increases and the angle (α) between vertical and horizontal normal force changes. By a careful design, a constant vertical force can be acquired by keeping $x*sin\alpha$ constant.

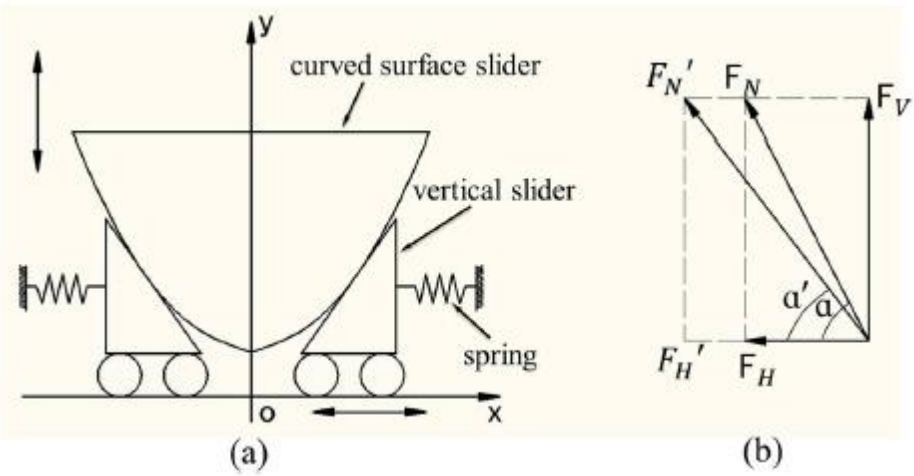

Figure 2.8 Curved surface slider mechanism

2.1.2. Compliant Constant Force Mechanisms

Rahman et all designed a curved beam (Figure 2.10) constant force mechanism [12] . The curved beams were approximated with variable spline curves with five interpolation points (Figure 2.9).

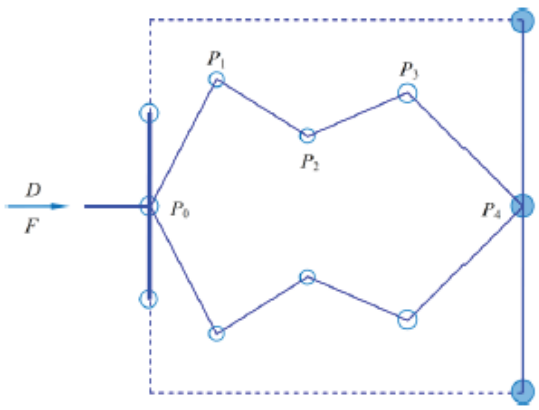

Figure 2.9 The Design Domain with interpolation points [12]

One of the chosen design and its deformed shape is in Figure 2.10. In the study 20 N force magnitude was aimed. At the interpolation points P_1, P_2, P_3, P_4 , 17.30 N, 19.02 N, 19.46

N, 20.00 N acquired respectively as in Figure 2.11. The whole domain is 100 mm and constant force is expected between the first 5 mm and 20 mm range of the mechanism.

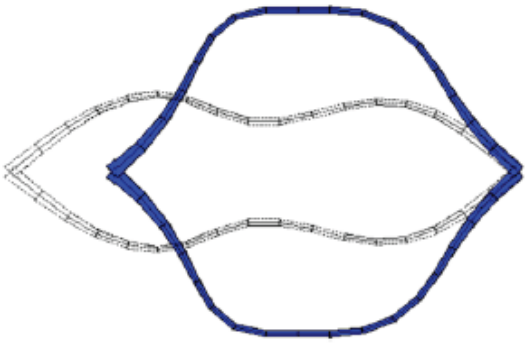

Figure 2.10 Curved beam model and its deformed shape [12]

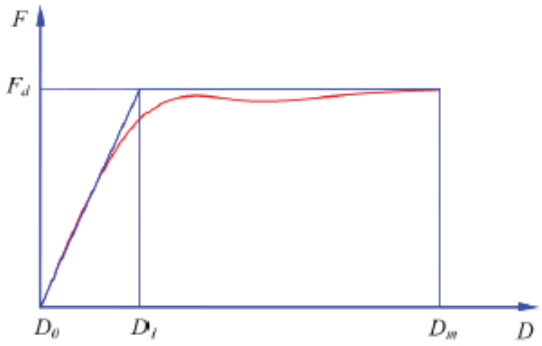

Figure 2.11 Force vs displacement for curved beam [12]

C. C. Lan [13] et all developed also a curved beam constant force mechanism (Figure 2.12) by distributed shape optimization. The design of the beam is inspired by the three coil spring mechanism in Figure 2.7.

Figure 2.12 The curved beam [13]

This mechanism requires 0.7 cm initial displacement and after that there is constant force region for the continuing 0.66 cm (Figure 2.13).

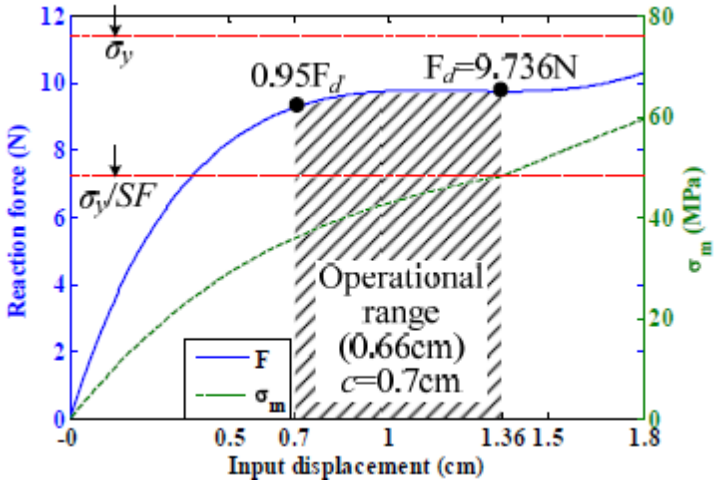

Figure 2.13 Force vs Displacement for curved beam [13]

The deflection of the flexible mechanism with respect to the given slider displacement is seen in Figure 2.14.

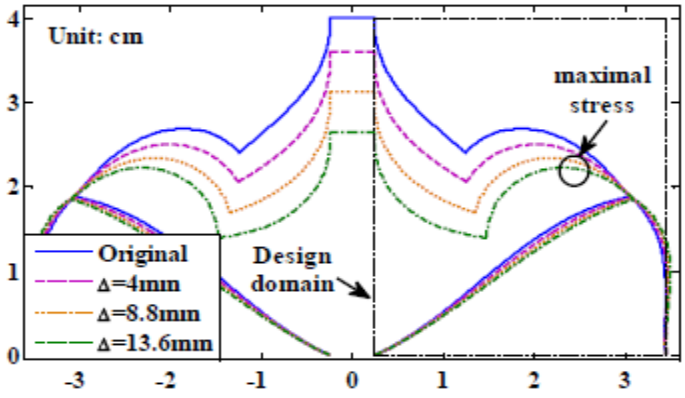

Figure 2.14 Deflected shape for curved beam [13]

2.1.3. Compliant Constant Force Slider Mechanisms

L.L. Howell et all [14] attained constant output force by compliant slider mechanisms. In Figure 2.15 compliant slider mechanism with three small length flexural pivots is given. The angles in pseudo rigid body model (PRBM) can be calculated by rigid body position analysis technique and output force (F) can be found by virtual work method. Since our thesis model is based on a compliant slider mechanism, going into more detail will be beneficial.

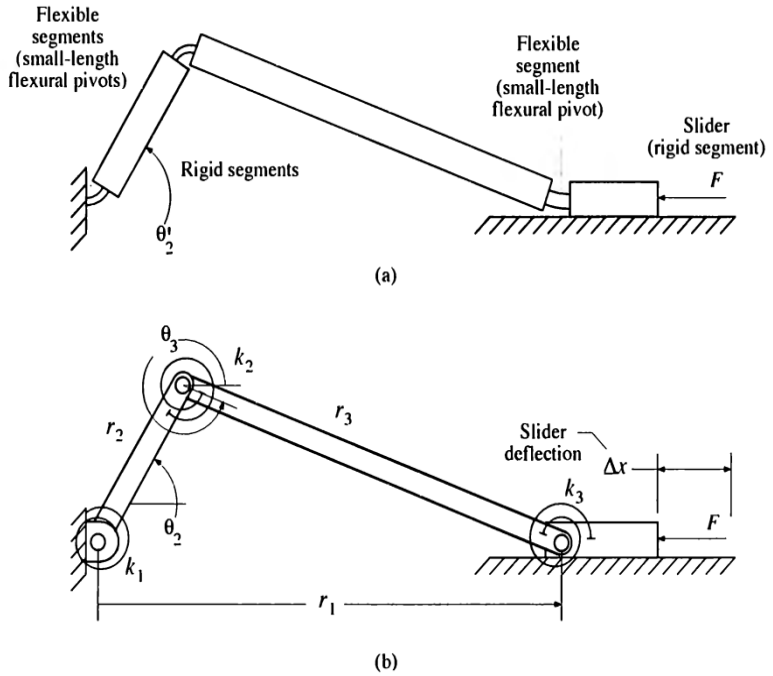

Figure 2.15 Compliant slider mechanism and its equivalent PRBM [14]

Fifteen versions of compliant slider mechanisms (Figure 2.16) were presented in [14]. These versions are divided into classes according to their joint positions and joint types. For example Class 1A is formed with a compliant segment at the end whereas Class 1B consists of revolute joints at the end and a compliant segment at the middle.

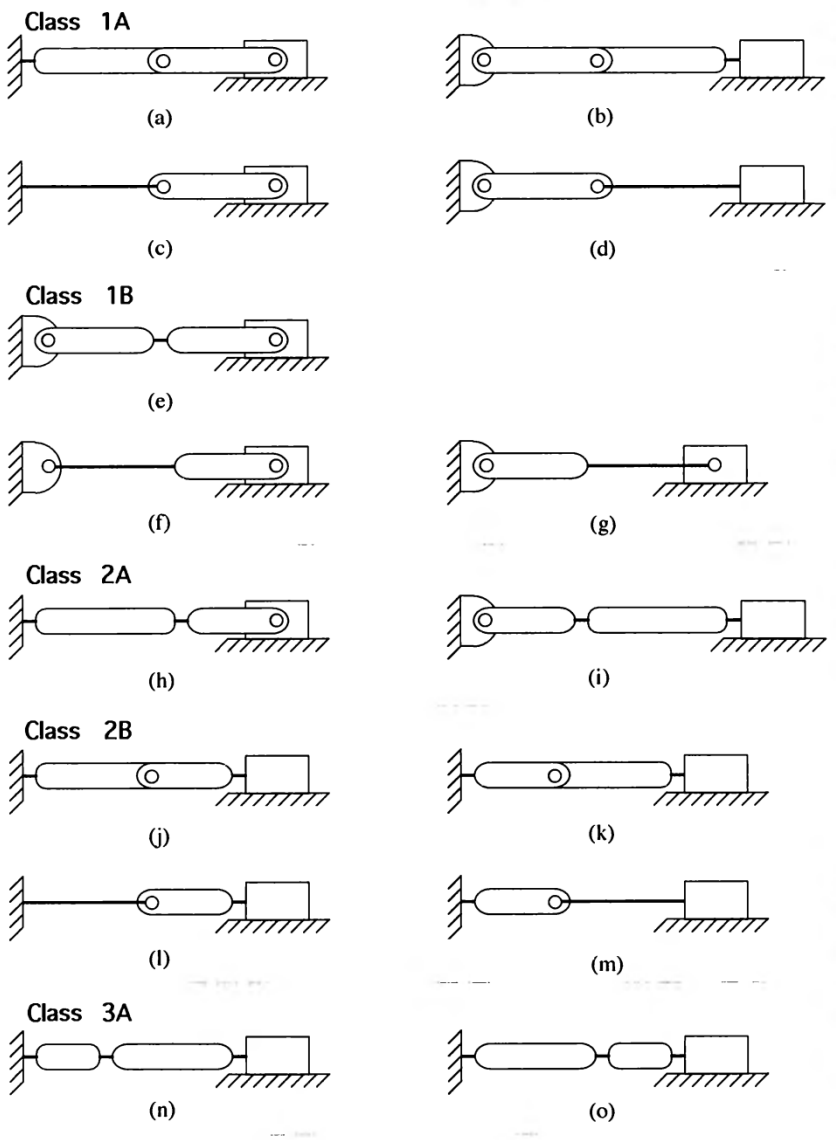

Figure 2.16 Fifteen versions of compliant slider mechanisms [14]

The optimization is made to find dimensions that obtain the minimum force variations for two ratios of stroke; %16 and %40. The ratio is the slider displacement divided by the total length of mechanisms. After non-dimensionalization process, some optimum mechanism parameters are presented in Table 2.1

Class	$\Delta x/(r_2+r_3)$	R	K_1	K_2	Ξ	Φ
1A	0.16	0.8274	—	—	1.0030	0.4537
	0.40	0.8853	—	—	1.0241	0.4773
1B	0.16	1.0000	—	—	1.0564	2.0563
	0.40	1.0000	—	—	1.1576	2.1513
2A	0.16	0.3945	0.1906	—	1.0015	0.9575
	0.40	0.4323	0.2237	—	1.0058	1.0466
2B	0.16	0.7591	—	0.1208	1.0721	1.2259
	0.40	0.8441	—	0.1208	1.1914	1.2154
3A	0.16	2.6633	1.0000	12.6704	1.0002	3.4016
	0.40	2.0821	1.0000	9.3816	1.0049	3.6286

Table 2.1 Non dimensionless results for constant force slider mechanisms

A sample is done here how to use the Table 2.1. For example for class 1A-a, for stroke=0.4 R=0.8853, force fluctuation ratio (Ψ) is 2.41%. Φ is a number to find F from dimensionless F'. If r_2=78.74 mm than r_3=78.74*0.8853=69.7 mm

Taking E=1655 Mpa, length of flexural pivot=5.08 mm width=12.7 h=0.76 mm

Then k_2=1655*12.7*$(0.76)^3$/5.08=151 N.mm/rad

$F=k_2*\Phi/r_2$=0.92 N average constant force magnitude with force fluctuation ratio of 2.41% throughout the stroke=0.4

The results in this reference are first confirmed with the design code at the appendix and after that with FEA software.

According to the design code, the average force F=0.9137 N as seen in Figure 2.17.

The details about the design code is in Chapter 4 and also FEA analysis procedure is elaborately explained in chapter 5. For the sake of completeness, the FEA results and design code results are given at this stage.

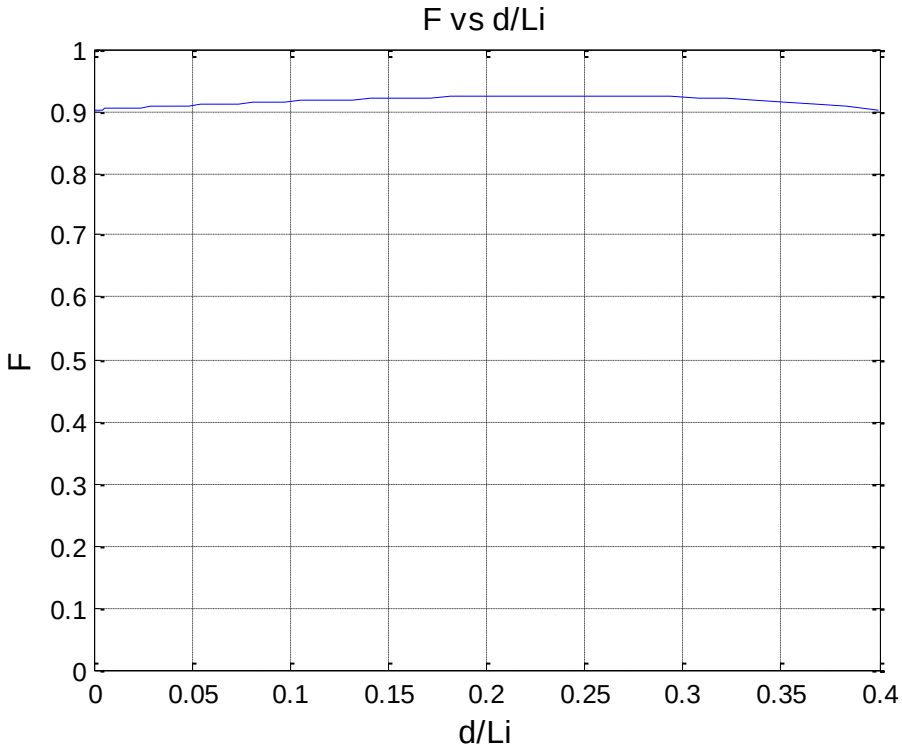

Figure 2.17 Force vs Stroke for Class 1A-a

The FEA result is presented in Table 2.2

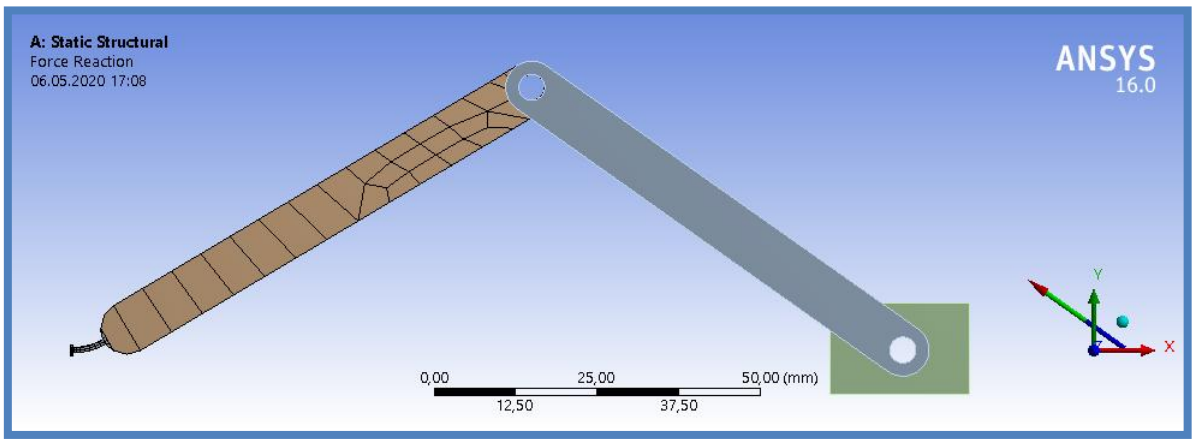

Figure 2.18 Geometry of class 1A-a

After 97 iterations (Figure 2.19), convergence is obtained.

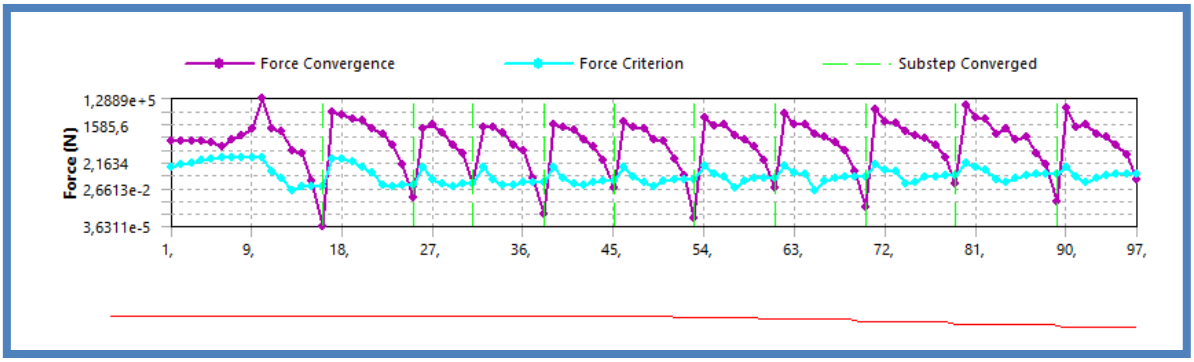

Figure 2.19 Solution details of Class 1-A-a

	Time [s]	Force Reaction (X) [N]
1	1,e-002	-0,98622
2	2,e-002	-0,98635
3	3,5e-002	-0,9861
4	5,75e-002	-0,98734
5	9,125e-002	-0,98814
6	0,14188	-0,98948
7	0,21781	-0,99133
8	0,33172	-0,99401
9	0,50258	-0,99762
10	0,75887	-1,0023
11	1,	-1,0053

Table 2.2 Force magnitudes for Class 1-A-a

In Table 2.2 Force magnitudes between 0.986-1.005 N are very close to the PRBM approach result 0.92 N.

Another sample from Table 2.1 is done for class 1A-c, for stroke=0.4 R=0.8853, force fluctuation ratio (Ψ) is 2.41% . Φ is a number to find F from dimensionless F'.

If r_2=168.7 mm than r_3=168.7*0.8853=149.3 mm

Take E=1655 Mpa, length of flexible beam is 203.2 mm, width is 12.7mm, h=3.18 mm

Than k_2=0.83*2.63*1655*12.7*(3.18)^3/12/203.2=610.1 N.mm/rad

$F=k_2*\Phi/r_2$=1.68 N average constant force magnitude with force fluctuation ratio of 2.41% throughout the stroke=0.4.

The results in this reference are first confirmed with the design code and after that with FEA software.

According to the design code, the average force F=1.67 N with force fluctuation 2.45% seen in Figure 2.20.

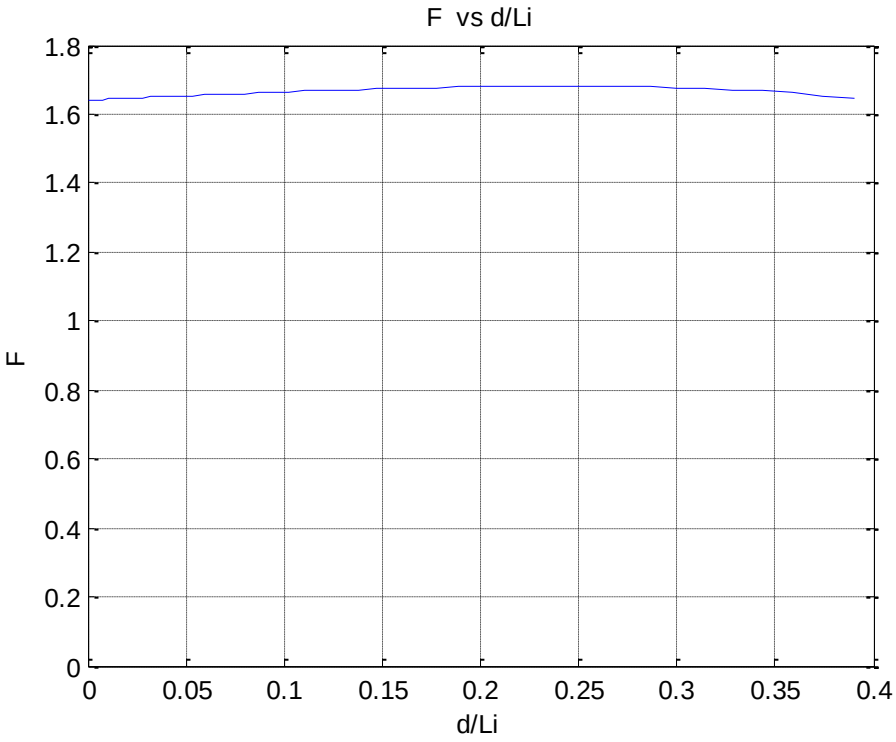

Figure 2.20 Force vs Stroke for Class 1A-c

The FEA results are presented below for class 1A-c.

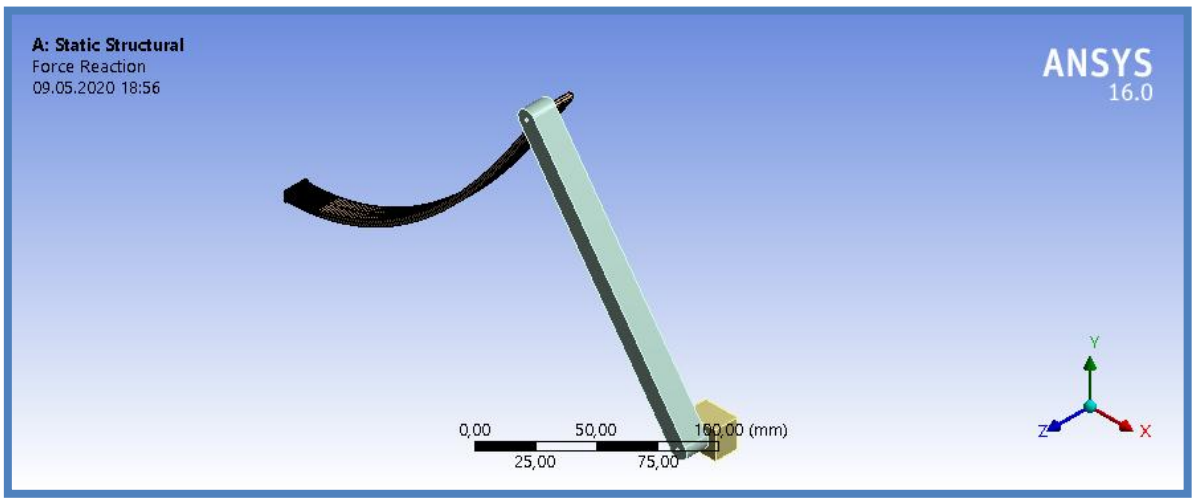

Figure 2.21 Geometry of class 1A-c

After 84 iterations (Figure 2.22), the problem is solved.

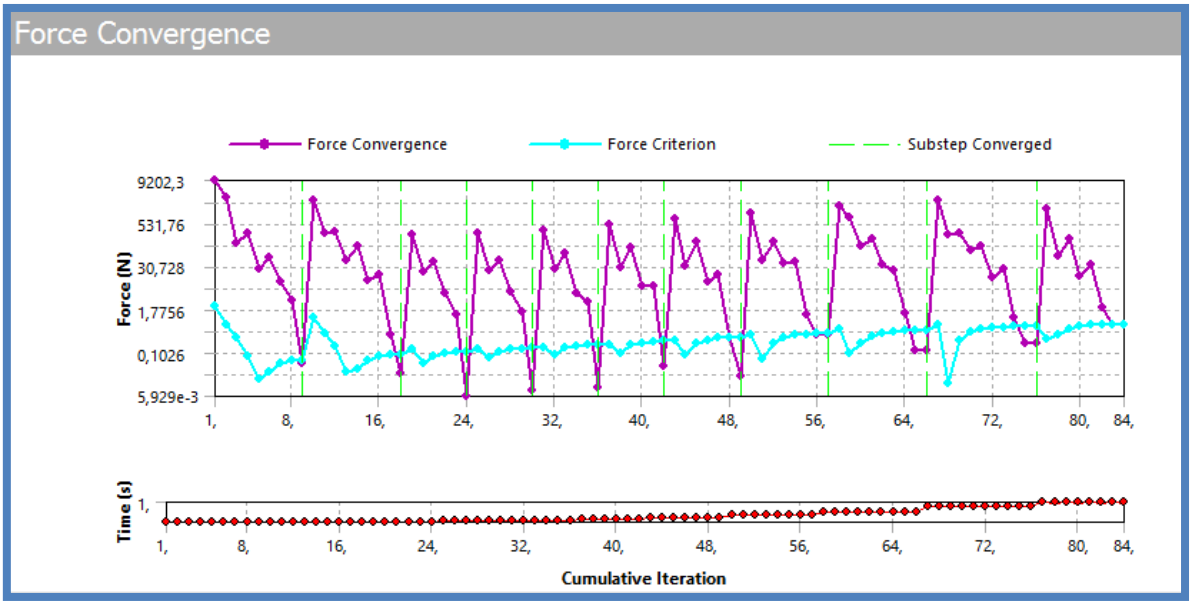

Figure 2.22 Solution details of Class 1-A-c

Tabular Data

	Time [s]	Force Reaction (X) [N]
1	1,e-002	-1,5768
2	2,e-002	-1,5805
3	3,5e-002	-1,584
4	5,75e-002	-1,5884
5	9,125e-002	-1,5942
6	0,14188	-1,6025
7	0,21781	-1,6141
8	0,33172	-1,6299
9	0,50258	-1,6493
10	0,75887	-1,6618
11	1,	-1,6387

Table 2.3 Force magnitudes for Class 1-A-c

In Table 2.3 Force magnitudes for Class 1-A-c between 1.57-1.66 N are very close to the PRBM approach result 1.67 N.

3. COMPLIANT MECHANISM ANALYSIS APPROACHES

3.1. Flexibility and Deflection

Compliant mechanisms generally need large deflection to have motion so rigid body assumption with no deformation is no longer valid. Since deflection of hinges is required for analysis and synthesis of compliant mechanisms, understanding the concepts such as stiffness, strength, rigidity, ductility and flexibility is essential.

Stiffness specifies how much a material bends or elongates due to a load whereas strength is limit stress prior to failure. Flexural rigidity (EI) is related to young's modulus and area moment of inertia. Similarly axial stiffness (EA) is a function of young's modulus and cross sectional area.

The fixed ended cantilever beam in the Figure 3.1 has dimensions *h* and *b*, *h* is greater than *b*. F_x is the applied load through the x dimension and F_y is in the direction of y axis. The maximum deflection in x and y directions is limited with the yield strength and the equations for maximum deflection are;

$$\delta_x = \frac{2 * Sy * L^2}{3 * E * b} \quad (3.1)$$

$$\delta_y = \frac{2 * Sy * L^2}{3 * E * h} \quad (3.2)$$

$$\frac{\delta_x}{\delta_y} = \frac{h}{b} \quad (3.3)$$

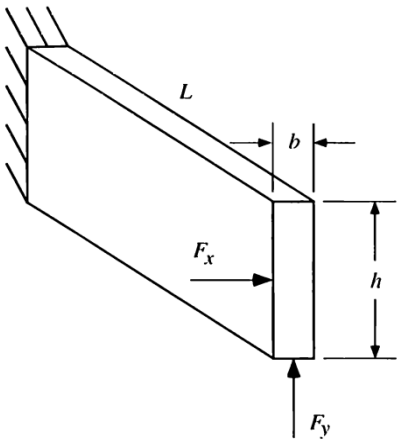

Figure 3.1 The cantilever Beam

h is greater than *b*, so the deflection in the x-direction is different and greater than the deflection in the y direction. This means, an isotropic cantilever beam has the same strength through all directions but has different deflections thereby different stiffnesses through different directions.

In compliant mechanism design generally the required deflection is known. For a specified deflection, if the maximum stress on the beam is over the safe limits, decreasing the thickness thus making the member less stiff or more flexible is beneficial to decrease the stress.

In rigid mechanisms, usually making the structural component more rigid is preferable to make them stronger and deflection is avoided because of the fatigue failure and vibration. However, in compliant mechanisms large deflection is requested. This deflection is preferred to be obtained with as small stress and load as possible.

Flexibility which is the opposite of rigidity is the ability of a mechanical element to deflect under load, supposing small deflection, the deflection (δ) is;

$$\delta=\frac{F*L^3}{3*E*I} \quad (3.4)$$

where the moment of inertia $I=\frac{b*h^3}{12}$ so,

$$\delta=\frac{4*F*L^3}{E*b*h^3} \quad (3.5)$$

As seen in Eq. (3.5), the deflection is affected by changing the material property thereby young's modulus or changing the dimensions. For example if L is doubled, the deflection is eight times greater, if h is halved the beam becomes eight times more flexible.

Usually flexibility and ductility is confused and used interchangeably. In fact a brittle material can be made very flexible by the geometry modifications. However, even brittle materials turn into a flexible manner, when the yield strength is passed it will fail suddenly. However a ductile material will not fail abruptly, only it will have some permanent deformation which is a signal for failure.

3.2. Pseudo Rigid Body Model

For analyzing compliant mechanisms which go into large deflections, nonlinear finite element method and elliptic integral solutions are precious instruments. However, these methods are more convenient for final tuning of a previously made rough initial design. To make the initial designs, a quicker and more practical way is needed. The pseudo rigid body method (PRBM) is a simple tool and efficient enough to provide the force deflection properties of a compliant mechanism.

When a cantilever beam is loaded with a force from its free end, the free end travels through an approximate circular path as shown in Figure 3.2. This near circular motion can be simulated by two rigid links which are connected by a revolute joint. The place of the joint is called characteristic pivot which is measured as a fraction of the beam's total length. The fraction coefficient is characteristic radius factor. The product of the beam length with the characteristic radius factor gives the pseudo rigid body link length. The angle between the flexible segment's initial undeflected position and PRBM link is pseudo rigid body angle (θ).

To model the beam's resistance to the applied load, a torsional spring is put at the characteristic pivot.

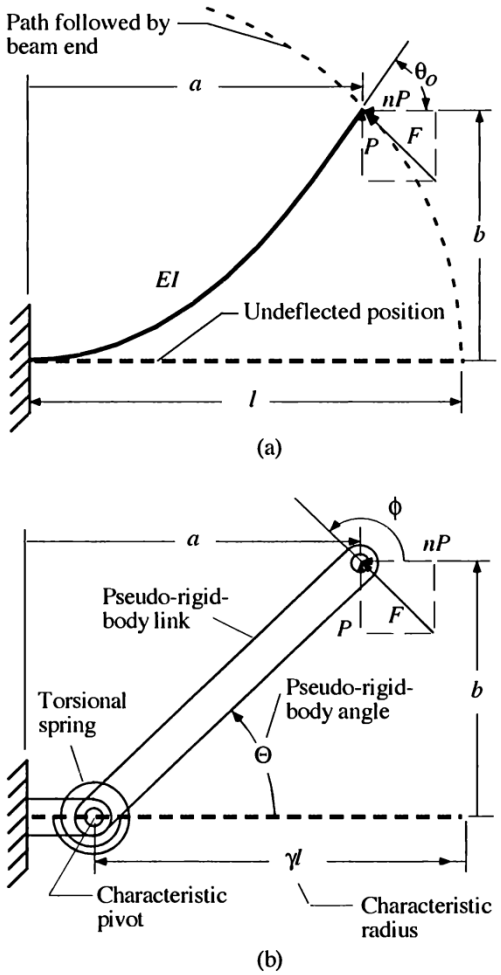

Figure 3.2 (a) Cantiveler beam loaded at free end (b) the pseudo rigid body model

3.2.1. Characteristic Radius Factor

The approximated circular path and thus link length for the applied load at the free end at various angles (n values) is found by multiplying the length of the beam and characteristic radius factor. The characteristic radius factor values are in the Figure 3.3. As observed for different n values γ doesn't change too much. Thus for the cases the mechanism moves and changing reaction force's angles at the free end, γ can be taken as 0.85 as average value [2].

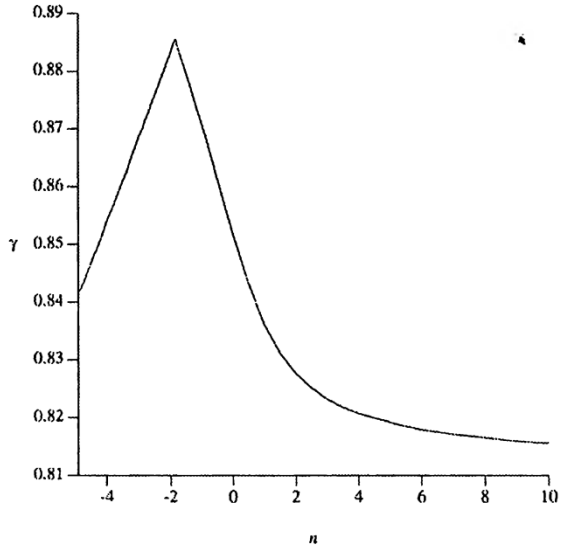

Figure 3.3 Charecteristic Radius Factor, Plot of γ vs n [2]

3.2.2. Stiffness Coefficient

The resistance of the beam is resembled by the torsional springs. The spring constant is to be approximated by stiffness coefficient non-dimensionless K_Θ values. As observed for different n values K_Θ does not vary too much. Thus for the cases the mechanism moves and changing reaction force's angles at the free end, γ can be taken as 2.65 as average value [2] .

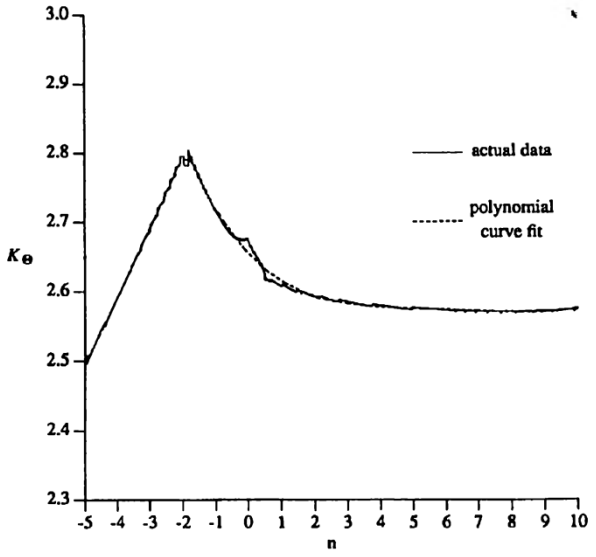

Figure 3.4 Stiffness Coefficient vs n [2]

3.2.3. Parameterization Limit

Pseudo Rigid Body Method is a parametric method that approximates the deflection and resistance of the compliant beams. There is a limit for parametric approximation for different n values. The limits for γ and K_Θ for different n values can be seen in Table 3.1. For example for n=0, γ=0.8517 and $K_\Theta = 2.67617$, PRBM can be used up to maximum pseudo rigid body angle Θ_{max}= 64.3 for γ and Θ_{max}=58.5 for K_Θ.

n	ϕ	γ	$\Theta_{max}(\gamma)$	c_θ	K_Θ	$\Theta_{max}(K_\Theta)$
0.0	90.0	0.8517	64.3	1.2385	2.67617	58.5
0.5	116.6	0.8430	81.8	1.2430	2.63744	64.1
1.0	135.0	0.8360	94.8	1.2467	2.61259	67.5
1.5	146.3	0.8311	103.8	1.2492	2.59289	65.8
2.0	153.4	0.8276	108.9	1.2511	2.59707	69.0
3.0	161.6	0.8232	115.4	1.2534	2.56737	64.6
4.0	166.0	0.8207	119.1	1.2548	2.56506	66.4
5.0	168.7	0.8192	121.4	1.2557	2.56251	67.5
7.5	172.4	0.8168	124.5	1.2570	2.55984	69.0
10.0	174.3	0.8156	126.1	1.2578	2.56597	69.7
-0.5	63.4	0.8612	47.7	1.2348	2.69320	44.4
-1.0	45.0	0.8707	36.3	1.2323	2.72816	31.5
-1.5	33.7	0.8796	28.7	1.2322	2.78081	23.6
-2.0	26.6	0.8813	23.2	1.2293	2.80162	18.6
-3.0	18.4	0.8669	16.0	1.2119	2.68893	12.9
-4.0	14.0	0.8522	11.9	1.1971	2.58991	9.8
-5.0	11.3	0.8391	9.7	1.1788	2.49874	7.9

Table 3.1 Numerical values for γ and K_Θ for different angles of force

3.3. Virtual Work Method

There are two methods to find the reaction forces at joints or fixed boundaries when loads are applied to a mechanism which consists of connected rigid bodies.

The first one is conventional free body diagram approach where force analysis is carried out by drawing each member's free body diagram. Then, equilibrium equations are implemented in all directions and system of linear equations which are results of the equilibrium equations are solved. By this method all reaction forces and moments at the joints can be obtained.

The other alternative is the virtual work method. Virtual work method may be very practical when all the reaction forces are not required. Especially while using PRBM approach, the existence and effects of torsional springs can easily be incorporated into virtual work approach [2].

A brief explanation of the method is done here. In Figure 3.5 (a) a downward force P is applied on point C and the wood between the slider and wall is compressed. If link AC is rotated clockwise virtually with angle δθ as shown in Figure 3.5 (b), assume that the mechanism moves with a small displacement. This motion is not real and only force P and Q does job. Because directions of the other reaction forces are not in the direction of the movement. For a static equilibrium condition, the total work done by the forces P and Q is zero. As a result an equation that directly relates P to Q can be written without determining the joint reaction forces.

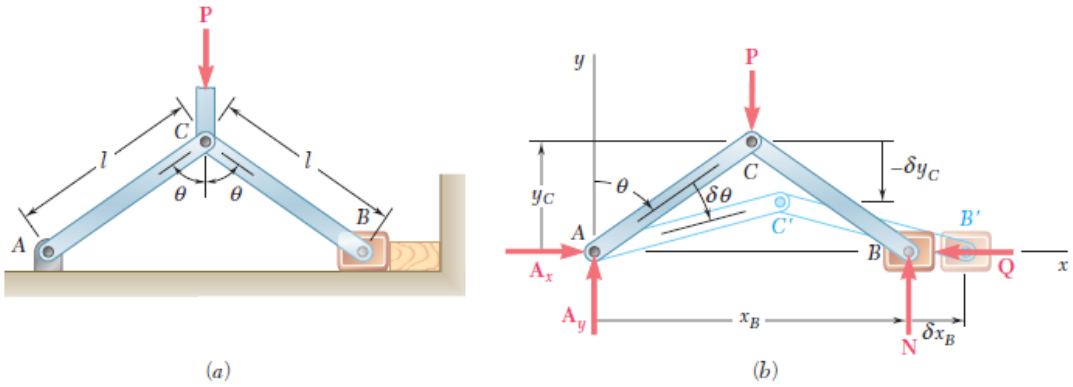

Figure 3.5 (a) Toggle vise; (b) Virtual movement of the toggle vise [15]

4. THE PROPOSED NOVEL CONSTANT FORCE MECHANISM

As mentioned in chapter 2, Howell [14] presented variations of compliant slider crank mechanisms which produce constant force at the slider. There are five basic groups depending on the joint and link types. Group 2B consists of two flexible parts with a joint in the middle. However, in this type one of these flexible segments must have small length flexural pivot.

In this study, we proposed a mechanism based on a compliant slider-crank mechanism which consists of four long compliant segments connected with two revolute joints as shown in Figure 4.1. To the best of our knowledge this type of constant force mechanism is not studied in the literature.

Generally, employing two long cascade beams is not suggested in order not to have wavy s like shapes. Because if the beams go into unpredictable, inflecting shapes, employing pseudo rigid body method would be inconvenient.

In the five basic groups presented [14], mechanisms possess straight links which have zero degree angle with the horizontal. To overcome the inflection problems, the idea of connecting the links initially angled with the horizontal comes to mind. The effect of initially angled beams orientation, link length ratio, spring constant ratio to be effective for maximizing constant force range and minimizing force magnitude fluctuation is studied. Moreover the effect of off-set distance (the vertical distance between slider and the fixed part of the link) is investigated.

In Figure 4.1 the design of thesis model is shown.

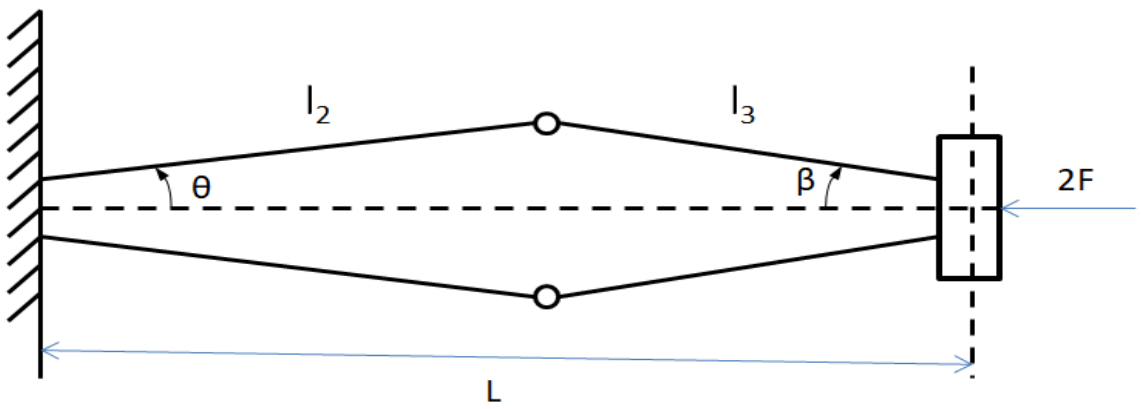

Figure 4.1 Design Model

Due to the symmetry, analyzing only the upper half of mechanism is sufficient (Figure 4.2).

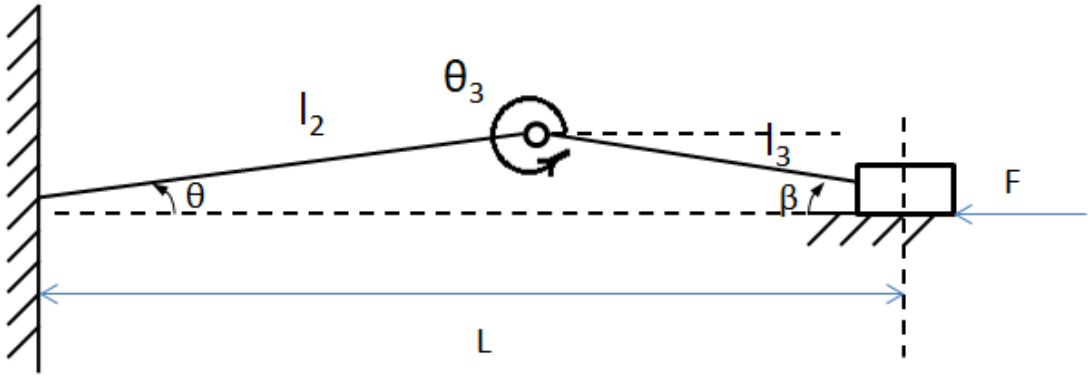

Figure 4.2 The upper half of the model

To analyze the compliant mechanism as a rigid body mechanism its PRBM is built as shown in Figure 4.3.

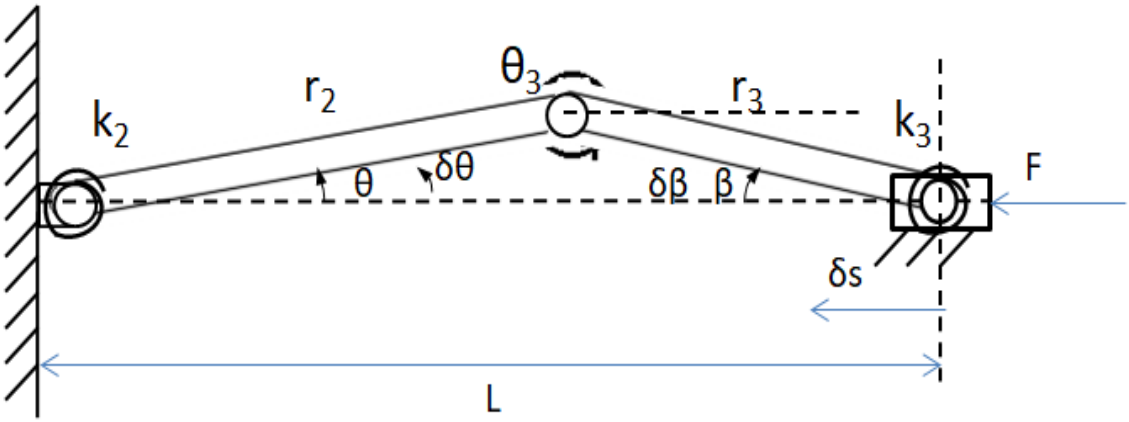

Figure 4.3 PRBM of the novel constant force mechanism

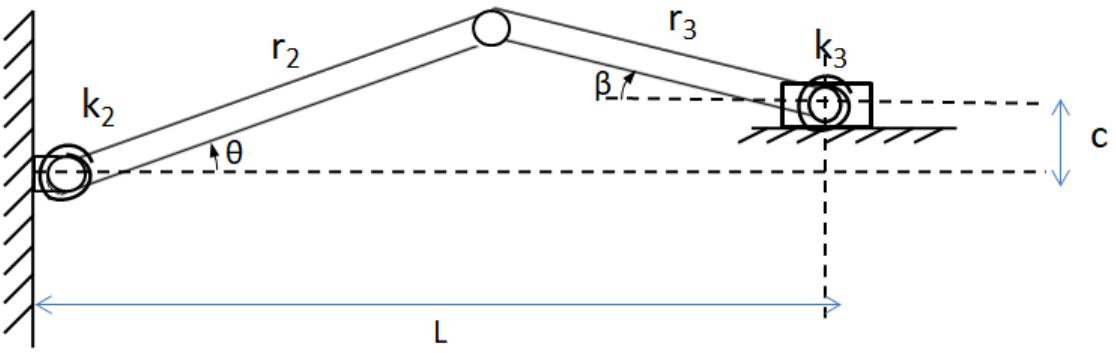

Figure 4.4 PRBM with eccentricity

Also to investigate the effect of eccentricity on force fluctuation, PRBM of the eccentric version is given in Figure 4.4.

Pseudo rigid link lengths, γ is the characteristic radius factor

$$r_2 = l_2 * \gamma \quad (4.1)$$

$$r_3 = l_3 * \gamma \quad (4.2)$$

s is stroke of the mechanism and can be calculated as

$$s = r_2 * \cos\theta + r_3 * \cos\theta_3 \quad (4.3)$$

$$c = r_2 * \sin\theta + r_3 * \sin\theta_3 \quad (4.4)$$

θ is the input thus to determine θ_3, rearranging Eq. (4.4)

$$r_3 * \sin\theta_3 = c - r_2 * sin\theta \quad (4.5)$$

where

$$\sin\theta_3 = (c - r_2 * \sin\theta)/r_2 \quad (4.6)$$

and

$$\theta_3 = asin((c - r_2 * \sin\theta)/r_2) \text{ (rad)} \quad (4.7)$$

Since arc sinus function has two roots, the correct value of θ_3 must be chosen attentively.

$$\theta_3 = -\beta \qquad (4.8)$$

Eq. (4.3) can be rewritten as

$$s = r_2 * \cos\theta + r_3 * \cos\beta \qquad (4.9)$$

By taking the derivative of Eq. (4.9):

$$\delta s = -r_2 * \sin\theta * \delta\theta - r_3 * \sin\beta * \delta\beta \quad (4.10)$$

To determine $\delta\beta$, Eq. (4.4) is to be rearranged;

$$c = r_2 * \sin\theta - r_3 * \sin\beta \qquad (4.11)$$

Taking the derivative with respect to θ of Eq. (4.11)

$$0 = r_2 * \cos\theta * \delta\theta - r_3 * \cos\beta * \delta\beta \qquad (4.12)$$

$$r_2 * \cos\theta * \delta\theta = r_3 * \cos\beta * \delta\beta \qquad (4.13)$$

$$\delta\beta = r_2 * \cos\theta * \delta\theta / (r_3 * \cos\beta) \qquad (4.14)$$

Substituting $\delta\beta$ into Eq. (4.10)

$$\delta s = -r_2 * \sin\theta * \delta\theta - r_3 * \sin\beta * \frac{r_2}{r_3} * \frac{cos\theta}{cos\beta} * \delta\theta \quad (4.15)$$

Simplifying Eq. (4.15)

$$\delta s = -r_2 * \sin\theta * \delta\theta - r_2 * tan\beta * cos\theta * \delta\theta \quad (4.16)$$

$$\delta s = -r_2 * (\sin\theta + tan\beta * cos\theta) * \delta\theta \quad (4.17)$$

According to the virtual work method, total virtual work for a static equilibrium equals to zero thus

$$w_{tot} = w_{springs} + w_{force} = 0 \qquad (4.18)$$

$$w_{springs} = w_{spring2} + w_{spring3} \qquad (4.19)$$

where,

$$w_{spring2} = -k_2 * (\theta - \theta_i) * \delta\theta \quad (4.20)$$

$$w_{spring3} = -k_3 * (\beta - \beta_i) * \delta\beta \quad (4.21)$$

Spring constant for links are

$$k_2 = \gamma * K_\theta * E * I/l_2 \qquad (4.22)$$

$$k_3 = \gamma * K_\theta * E * I/l_3 \qquad (4.23)$$

In order to simplify the analysis procedure and due to the varying position, an average characteristic radius factor (γ) value can be used; γ =0.85

K_θ is average value of stiffness coefficient from; K_θ=2.65

I is moment of inertia, E is modulus of elasticity

$$w_{force} = -F * -\delta s \quad (4.24)$$

Substituting Eqns. (4.20-21-22) into Eq.(4.18)

$$F * \delta s = -k_2 * (\theta - \theta_i) * \delta\theta - k_3 * (\beta - \beta_i) * \delta\beta \quad (4.25)$$

Substituting Eq.(4.17) into Eq. (4.24) to take derivatives with respect to $\delta\theta$

$F * r_2 * (\sin\theta + tan\beta * cos\theta) * \delta\theta = k_2 * (\theta - \theta_i) * \delta\theta + k_3 * (\beta - \beta_i) * r_2 *$

$\cos\theta * \delta\theta/(r_3 * \cos\beta)$ (4.26)

After simplifications we obtain

$F * r_2 * (\sin\theta + tan\beta * cos\theta) = k_2 * (\theta - \theta_i) *+ k_3 * (\beta - \beta_i) * r_2 * \cos\theta/(r_3 * \cos\beta)$

(4.27)

Eq. (4.27) is the base equation to determine reaction force *F* at the slider. To obtain *F* and provide the constant force region, there are six structure parameters (r_2, r_3, $k_2, k_3, \theta_i, \beta_i$). In order to lessen the structure parameters for design charts, we can convert Eq. (4.27) to a non-dimensionless form.

To obtain non-dimensionalized form for generalization, the following procedure can be used:

Dividing Eq. (4.27) by r_2

$$F * (\sin\theta + tan\beta * cos\theta) = k_2/r_2 * (\theta - \theta_i) *+ k_3/r_3 * (\beta - \beta_i) * \cos\theta/\cos\beta \quad (4.28)$$

Multiplying Eq. (4.28) by r_3

$$F * r_3 * (\sin\theta + tan\beta * cos\theta) = k_2 * \frac{r_3}{r_2} * (\theta - \theta_i) + k_3 * (\beta - \beta_i) * \cos\theta/\cos\beta \quad (4.29)$$

Dividing Eq. (4.29) by k_2

$$F * \frac{r_3}{k_2} * (\sin\theta + tan\beta * cos\theta) = \frac{r_3}{r_2} * (\theta - \theta_i) + \frac{k_3}{k_2} * (\beta - \beta_i) * \frac{cos\theta}{\cos\beta} \quad (4.30)$$

Defining, unitless F'as

$$F' = F * \frac{r_3}{k_2} \quad (4.31)$$

Unitless link length ratio is

$$R = \frac{r_3}{r_2} \quad (4.32)$$

Unitless spring constant ratio is

$$K = \frac{k_3}{k_2} \quad (4.33)$$

Now Eq. (4.29) becomes

$$F' * (\sin\theta + tan\beta * cos\theta) = R * (\theta - \theta_i) + K * (\beta - \beta_i) * \frac{cos\theta}{\cos\beta} \quad (4.34)$$

which is the main dimensionless formula. There are four design parameters (R, K, θ_i, β_i).

4.1. 3D Design Charts

4.1.1. Case 1

After constituting the general formula, the code given at the Appendix related with Eq. (4.34) is formed in a mathematics software. Generating 3D design charts eases to visualize and determine roughly where F' has the maximum constant force range and minimum force magnitude variation.

Explanation of 3D design charts is done via a sample in Figure 4.5. This sample value set is one of the optimum results that obtained from the code (Table 4.1).

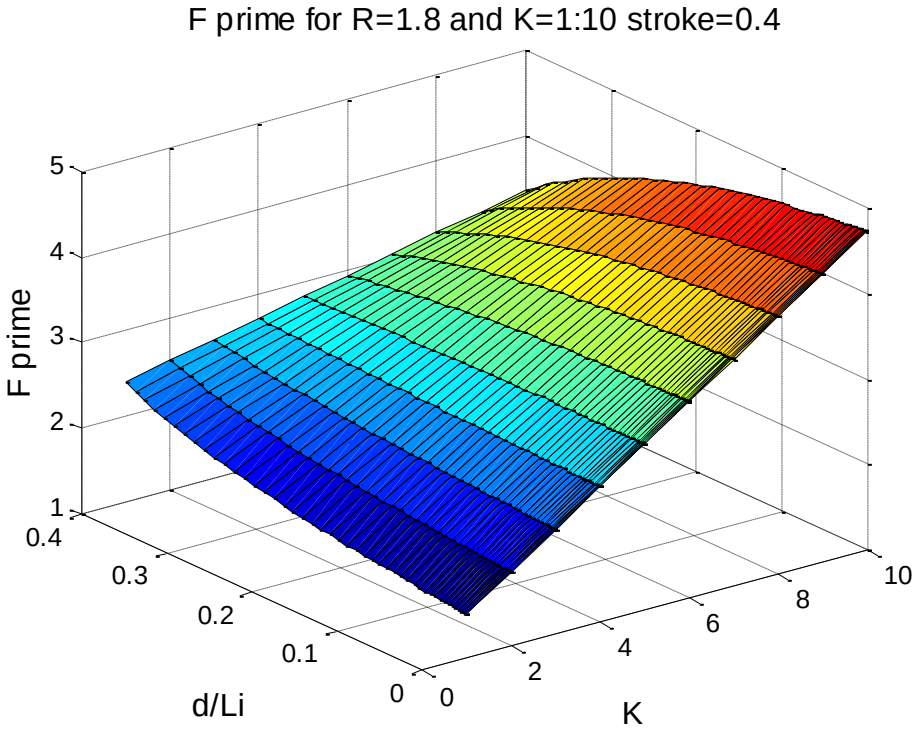

Figure 4.5 3D design chart of data set 1

Parameter	Value	Unit
l_2	100	mm
l_3	180	mm
R	1.8	
θ_i	0	degree
β_i	0	degree
h	5	mm
w	1	mm

Table 4.1 Optimum parameter values Case-1

We only have three axes and must assign two of them to *F*' and stroke (d/L_i) in order to visualize the constant force regions. In stress free beginning conditions β_i is related to θ_i and can easily be calculated by with respect to θ_i. Thus design parameters finally reduce to three (R, K, θ_i). If required, β_i can be different from the corresponding value of θ_i in the pre-stressed connections. However, in this thesis work, initially stress free conditions are examined.

This optimization process is challenging, even we restricted the design to the three design parameters. We have left only one axis for three design parameters, so *K* is chosen for this available axis. As seen in 3D design chart of case-1 (Figure 4.5) y axis is chosen to investigate the constant force region for *K* values for a range between 1 and 10. First, a long trial and error procedure starts with different *R* values. After converging to a specified *R* value which is 1.8 for the dataset-1, detailed 2D plot inspection begins to find the stroke and force fluctuation ratio.

In our study, two kinds of data set will be mentioned. In the first case as in dataset-1, θ_i and β_i are equal to zero and the links are initially stress free. As the effect of changing θ_i will be discussed in the upcoming sections, if θ_i is zero, for different link ratios and spring constants, generally force fluctuation is minimum and stroke of constant force turns out to be maximum. Also constant force starts from the beginning of the slider stroke. However for two long beams when θ_i selected as zero, inflection problems which yields extreme error in PRBM. This inflecting s-shape problem risk is only at the beginning of the slider movement. Thus by initially displacing the slider by only a small displacement in the compression direction mechanically, the inflection problem should be overcome. The stroke loss from the initial displacement of the slider is negligible since it is only moved for a negligible displacement. Thus it can be assumed as full stroke practically.

l_2 and l_3 values are chosen first heuristically and converged to a specified range. As link 2 is fixed from the left end and link 3 is connected to the slider directly without a joint, the motion is basically generated through the deflection of the beams in the mechanism. Thus choosing link 2 and link 3 lengths close to each other is convenient. If length of the links varies too much, the small link would have a dramatic stress increase during the motion.

h and *w* values are needed to calculate *F* value from *F′* via Eq. (4.31) and can be selected any values due to the corresponding moment of inertia ratio. As a general rule of thumb, while deciding the numerical values of the design parameters, *h* should not be too much

not to decrease the flexibility as the mechanisms moves through the deflection of links. Also, both of the values can be optimized according to the force magnitude needed and stress value limits. For example if a compliant link reaches stress limits, without changing the moment of inertia ratio, *h* can be decreased and *w* can be increased. By this change, for the same deflection levels, lower stress values can be encountered.

As observed in Figure 4.5, the vertical z column is the F' value from Eq. (4.34). The y axis is *K* value which is unitless spring constant ratio in Eq. (4.33), spring constant values, k_2 and k_3 are functions of modulus of elasticity (*E*) and moment of inertia (*I*) Eq. (4.22-23). As the material is same and isotropic for both beams, *E* does not influence *K* however has an effect on stress values encountered at beam and the reaction force *F*. Therefore to change the *K* value, the only parameter remains moment of inertia. Thus width and height values from Eq. (4.36) become determinant which can be altered for different values for both beams.

Initial total length of PRBM of the mechanism is

$$L_i = r_2 * \cos\theta_i + r_3 * \cos\beta_i \quad (4.35)$$

$$I = \frac{w*h^3}{12} \quad (4.36)$$

$$d = L_i - s \quad (4.37)$$

$$\psi = \left(\frac{F_{max}}{F_{min}} - 1\right) * 100 \quad (4.38)$$

The x axis is d/L_i value, which is the ratio of the distance travelled by the slider over the total initial length of the PRBM of the mechanism. Distance travelled by the slider is calculated by subtracting the instantaneous length of the PRBM of the mechanism while moving (Eq. (4.4)) from the total initial length of the pseudo rigid body of the mechanism (Eq. (4.35)). d/L_i value is a dimensionless quantity that gives the ability to compare different mechanisms for their constant force strokes independent from the link lengths.

3D plots gives the ability to observe different spring constant ratios while link lengths and initial angles are kept at specified values.

As 3D Figure 4.5 is examined, between K = 4 and 6 value a constant force zone can be observed roughly. To ensure the maximum constant force range, trying for K values around 5 by increments or decrements.

In Table 4.2 for different K values, for a stroke (d/L_i)= 0.4, force fluctuation ratio is listed. Force fluctuation ratio (ψ) is F_{max} over F_{min} in Eq. (4.38) calculated for 50 evenly spaced pseudo rigid body angle θ through the displacement of slider. As observed, for θ_i=0, ψ is minimum with the value of 0.77% for K=4.5.

K	For θ_i=0, ψ (%)
4.0	5.41
4.3	2.44
4.4	1.5
4.5	0.77
4.6	0.91
4.7	1.61
4.8	2.37
5.0	3.94
5.1	4.74
5.5	8.92

Table 4.2 Various K values for data set 1 θ_i =0

K values are checked by the help of the code at the appendix and also by taking out 2D slice (Figure 4.6) from 3D plot to visualize the results and compare them quickly. For K=4.5, ψ with 0.77% is nearly a constant line for the whole stroke. At 2D sketches, F is at the vertical axis instead of F′ in order to check the actual values with the FEA software. Actually F value is F′ multiplied by a constant. As mentioned, h = 1 and w = 5 are taken for calculating F values.

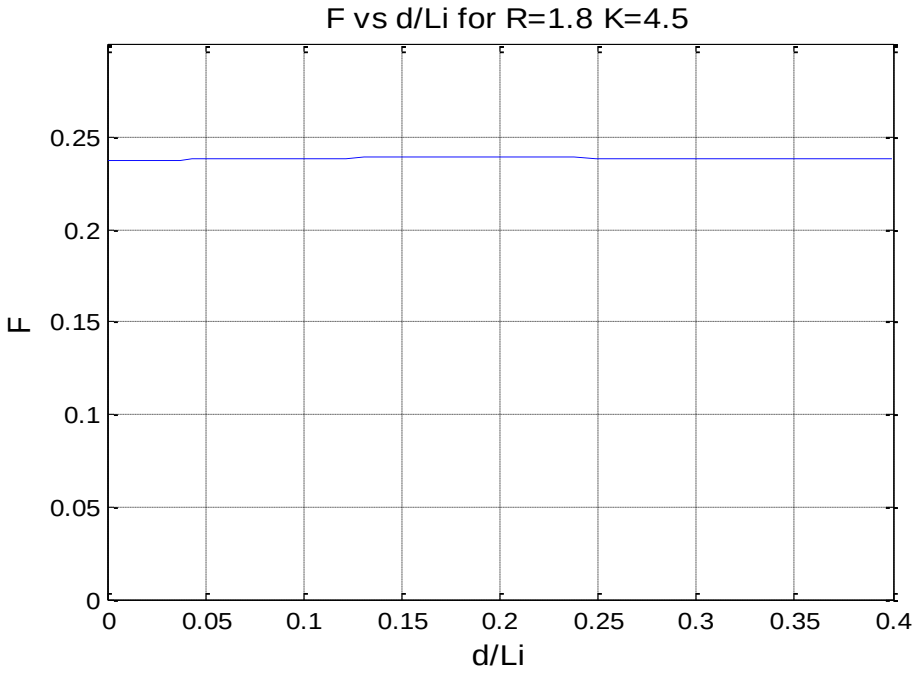

Figure 4.6 2D plot of data set-1

θ_i is started from 0 degree and incremented by evenly spaced 50 points up to 80 degrees during the motion of the slider for the 40% of the initial PRBM length. The F values vs d/L_i in Figure 4.6 is given in Table 4.3

d/Li	F	d/Li	F
0,000	NaN	0,131	0,2391
0,000	0,2374	0,141	0,2391
0,001	0,2374	0,151	0,2392
0,002	0,2374	0,161	0,2392
0,004	0,2375	0,171	0,2392
0,006	0,2375	0,182	0,2392
0,008	0,2375	0,193	0,2392
0,011	0,2376	0,204	0,2392
0,014	0,2377	0,215	0,2392
0,018	0,2377	0,226	0,2391
0,022	0,2378	0,238	0,2391
0,027	0,2379	0,249	0,2390
0,032	0,2380	0,261	0,2389
0,037	0,2380	0,272	0,2389
0,043	0,2381	0,284	0,2388
0,049	0,2382	0,296	0,2387
0,056	0,2383	0,308	0,2386
0,063	0,2384	0,319	0,2385
0,070	0,2385	0,331	0,2384
0,078	0,2386	0,343	0,2384

0,086	0,2387	0,354	0,2384
0,094	0,2388	0,366	0,2384
0,103	0,2389	0,377	0,2384
0,112	0,2389	0,389	0,2386
0,121	0,2390	0,400	0,2388

Table 4.3 F and d/L_i for data set-1

Another way of overcoming s-shape problem is connecting link-2 initially angled with the fixed part. θ_i is selected very close to zero in order to prevent inflection of links. As θ_i converges to zero the constant force fluctuation becomes minimum and range of constant force turns out to be maximum. The trials in the FEA software showed that if θ_i is below 0.05 degrees which is a very small number, the mechanism doesn't work and has inflection. Thus giving θ_i= 0.05 and looking for the same *K* values and the fluctuation ratios will be beneficial (Table 4.4). At around K=4.8, force fluctuation is minimum. Even giving a very small initial angle has increased force fluctuation. The effect of θ_i will also be studied in detail in the next section.

K	For θ_i=0.05, Ψ (%)
4.0	8.57
4.3	5.5
4.4	4.54
4.5	3.75
4.6	3.53
4.7	3.36
4.8	3.22
5.0	3.83
5.1	4.62
5.5	7.79

Table 4.4 Different K values for data set 1 θ_i =0.05

4.1.2. The effect of θ_i

After deciding K=5 and for R=1.8 with a maximum fluctuation ratio of 3.7 %, changing θ_i values starting from 0 to 10° is beneficial to understand the effect of teta initial to the constant force range.

As it is summarized at and seen in Figures 4.7-4.14, constant force stroke decreases for an increasing θ_i. For the final value θ_i=10, the constant force region is a minumum. θ value in which the mechanism gets into the constant force zone is 55.75 degree. Also, with increasing θ_i values the entrance into the constant force range delays. θ_i=0 has very pleasant outcomes for constant force range theoretically, but as a result of the trials at the crosscheck part via finite element method, at θ_i values below 0.05 degrees, the compliant segments tend to inflect.

θ_i	Constant Force Range	θ at the start and finish of constant force zone
0	0.4	0-80
0.5	0.3915	10-80
1	0.3778	16.25-80
2	0.3505	24.5-80
3	0.3258	30.25-80
4	0.3022	35-80
5	0.2817	38.75-80
10	0.1734	55.75-80

Table 4.5 Constant force ranges with respect to θ_i for data set 1

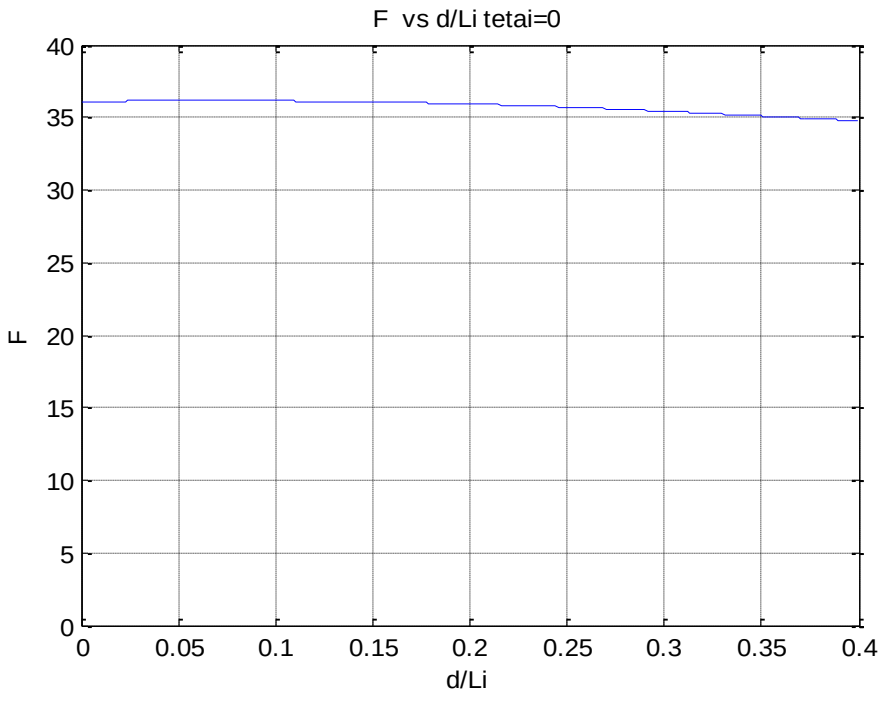

Figure 4.7 F vs d/L_i for data set 1 with θ_i=0

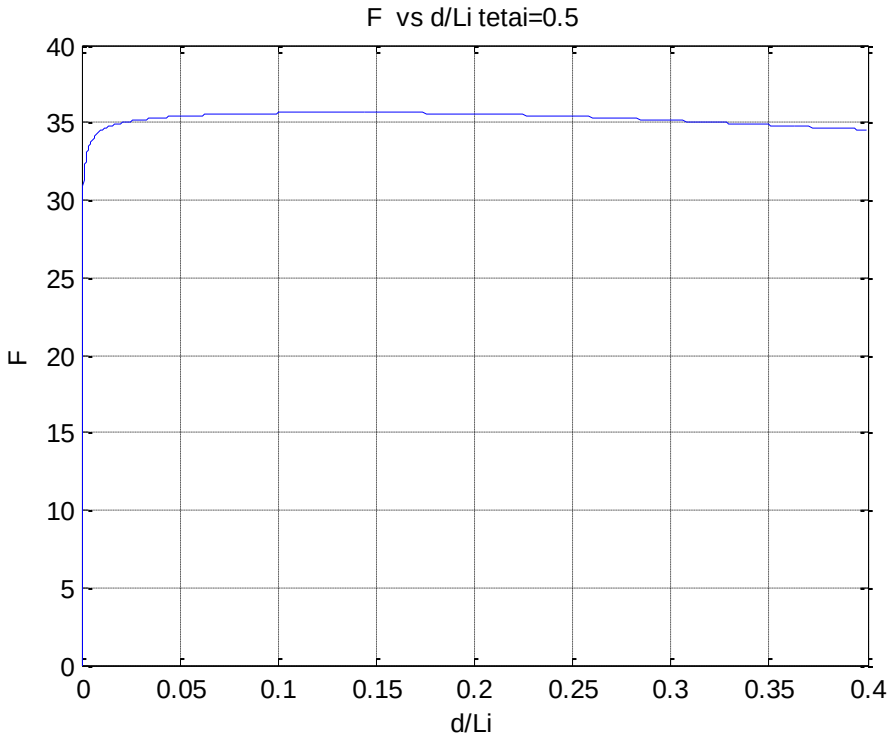

Figure 4.8 F vs d/L_i for data set 1 with θ_i=0.5

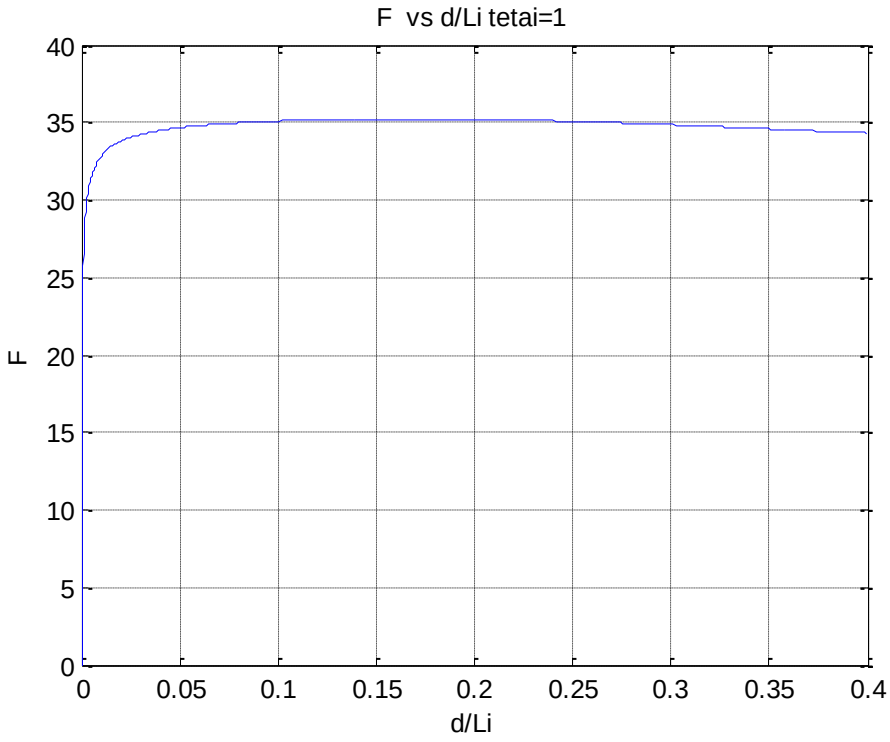

Figure 4.9 F vs d/L_i for data set 1 with θ_i=1

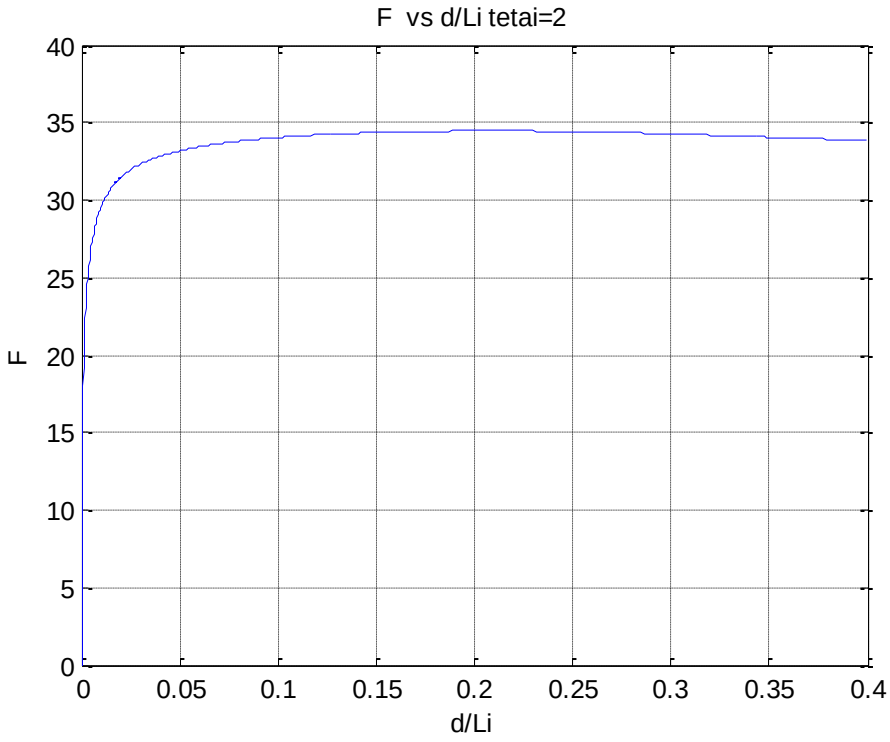

Figure 4.10 F vs d/L_i for data set 1 with $\theta_i=2$

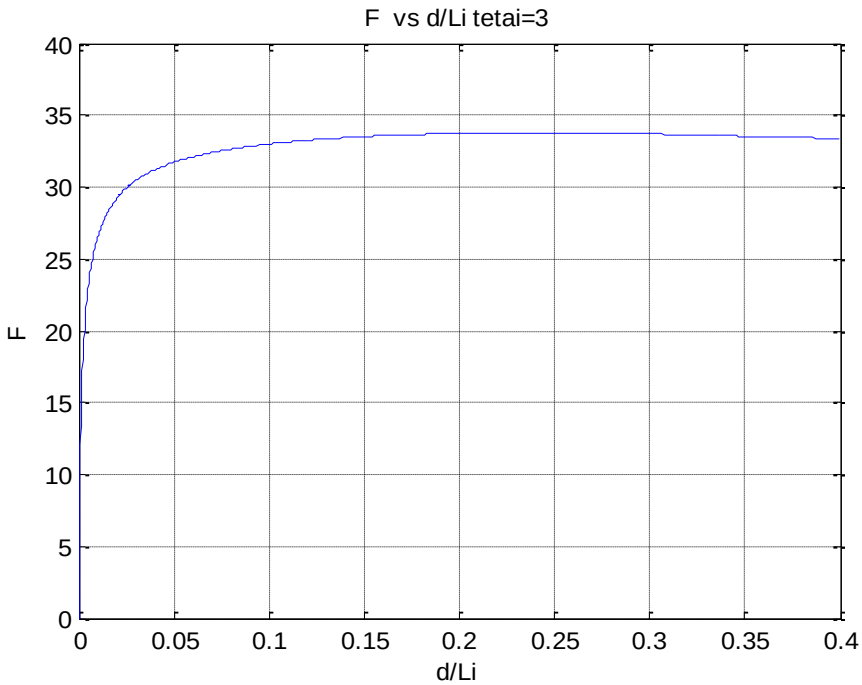

Figure 4.11 F vs d/L_i for data set 1 with $\theta_i=3$

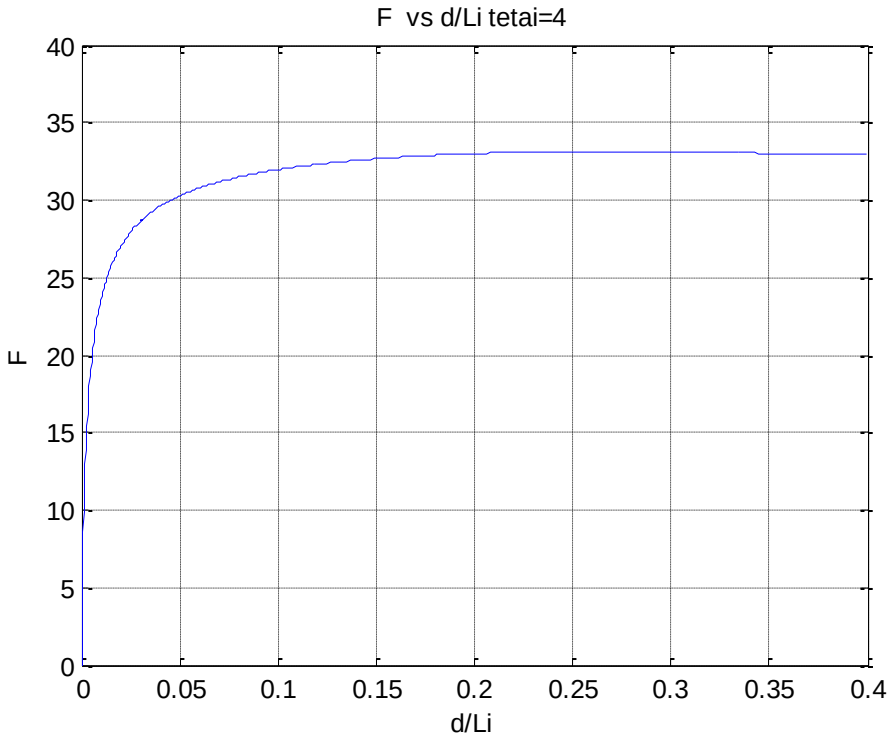

Figure 4.12 F vs d/L_i for data set 1 with θ_i=4

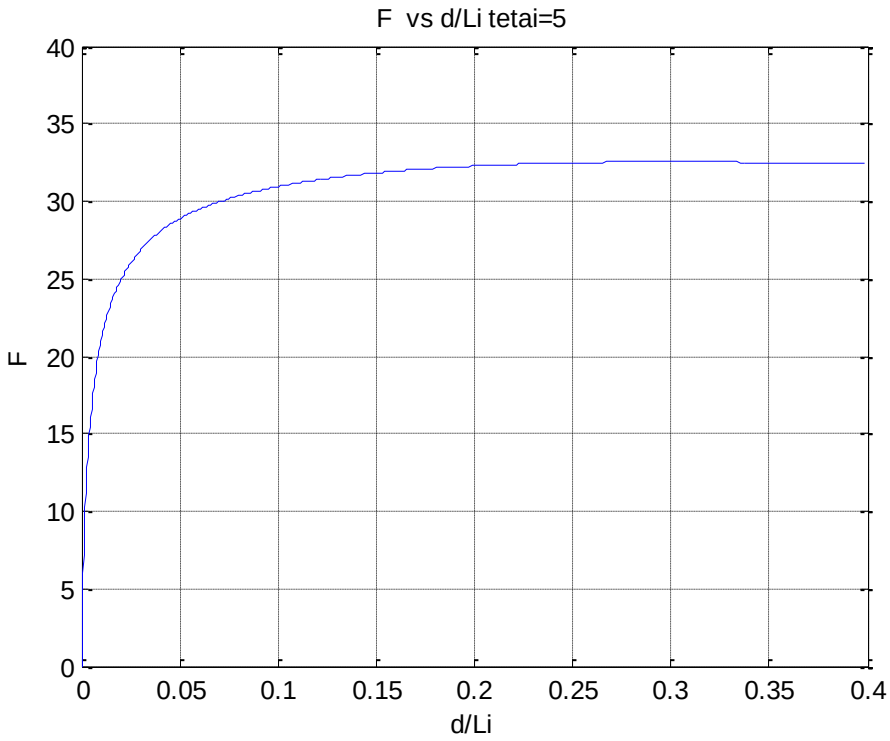

Figure 4.13 F vs d/L_i for data set 1 with θ_i=5

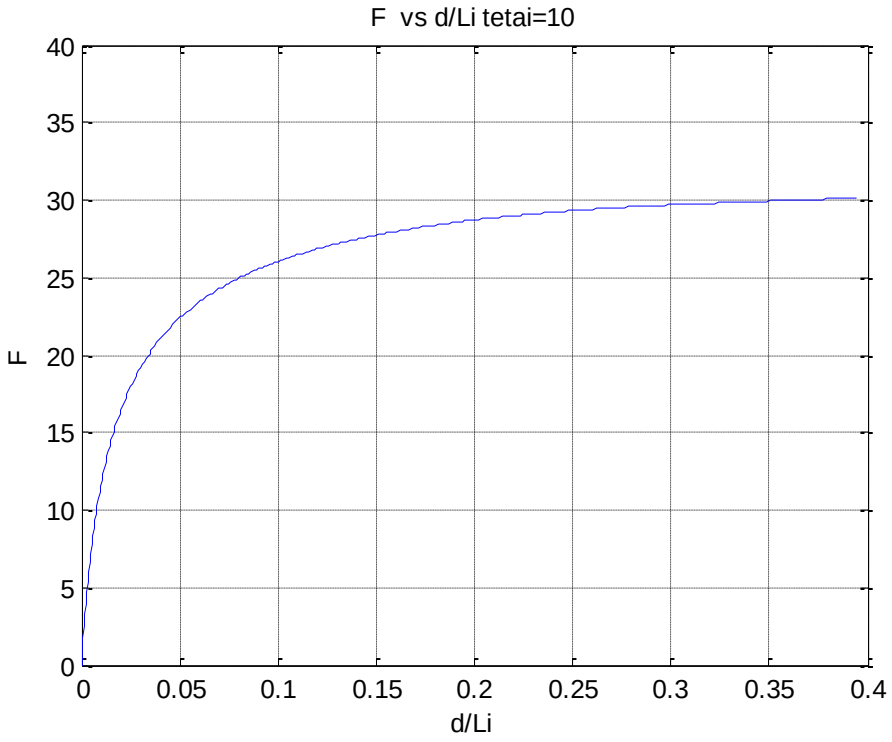

Figure 4.14 F vs d/L_i for data set 1 with θ_i=10

4.1.3. The effect of Off-Set Parameter

For data-set 1, the results of giving an off-set both in the positive or negative direction for dataset-1 reduces constant force quality as observed at the figures (4.14-18).

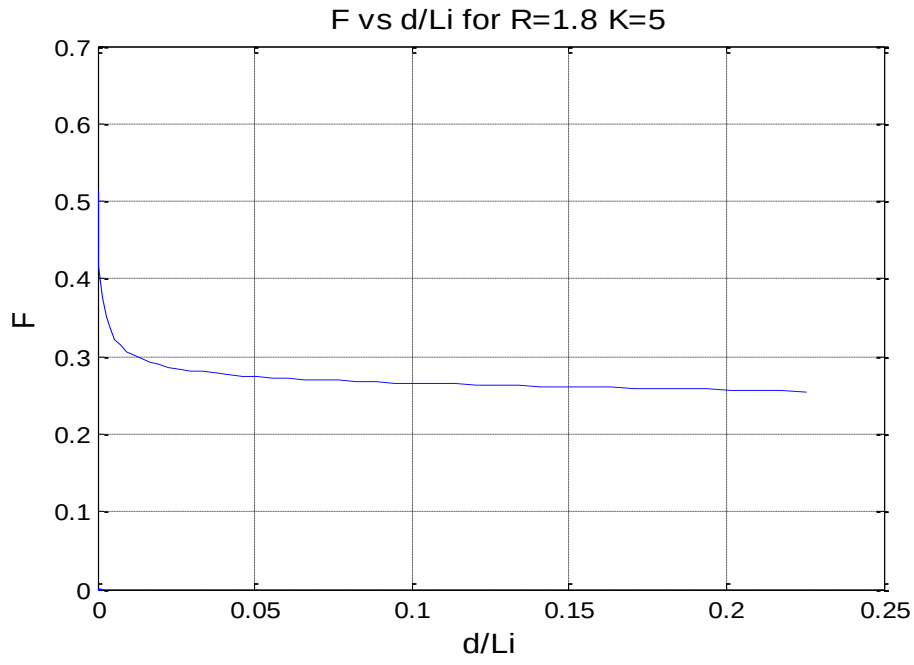

Figure 4.15 F vs d/L_i for data set 1 with θ_i=0.05, off-set 10 mm

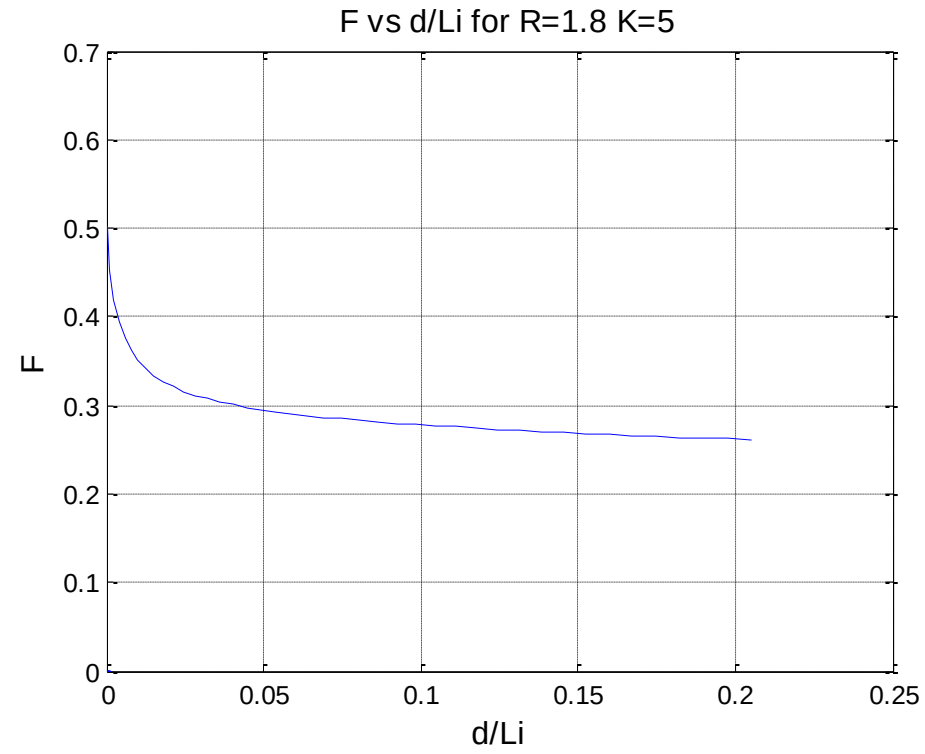

Figure 4.16 F vs d/L_i for data set 1 with θ_i=0.05, off-set 20 mm

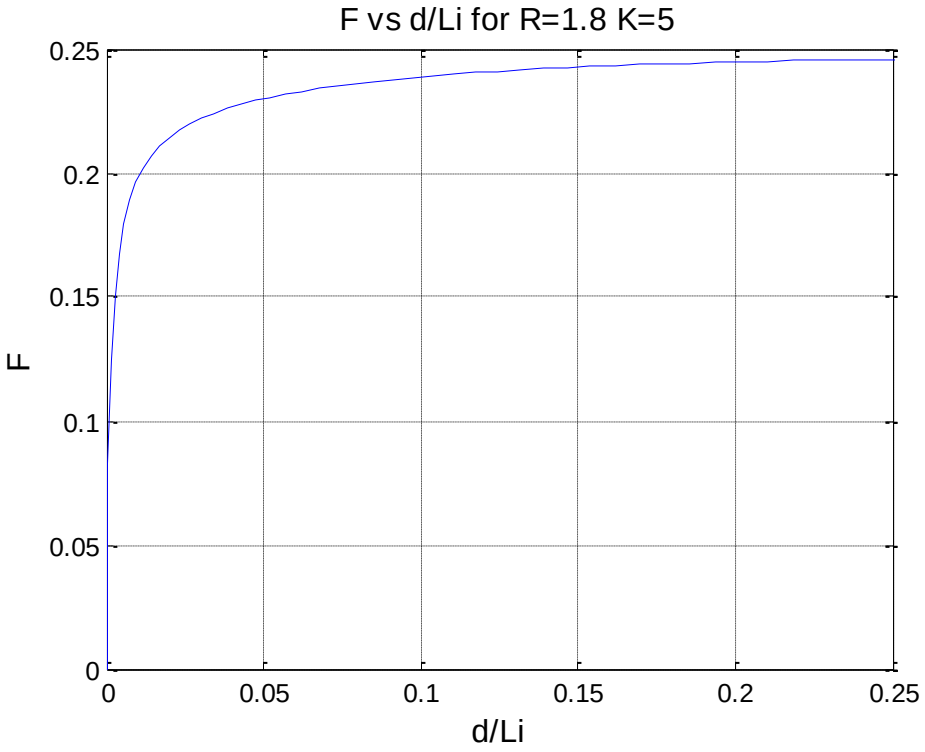

Figure 4.17 F vs d/L_i for data set 1 with θ_i=0.05, off-set -10 mm

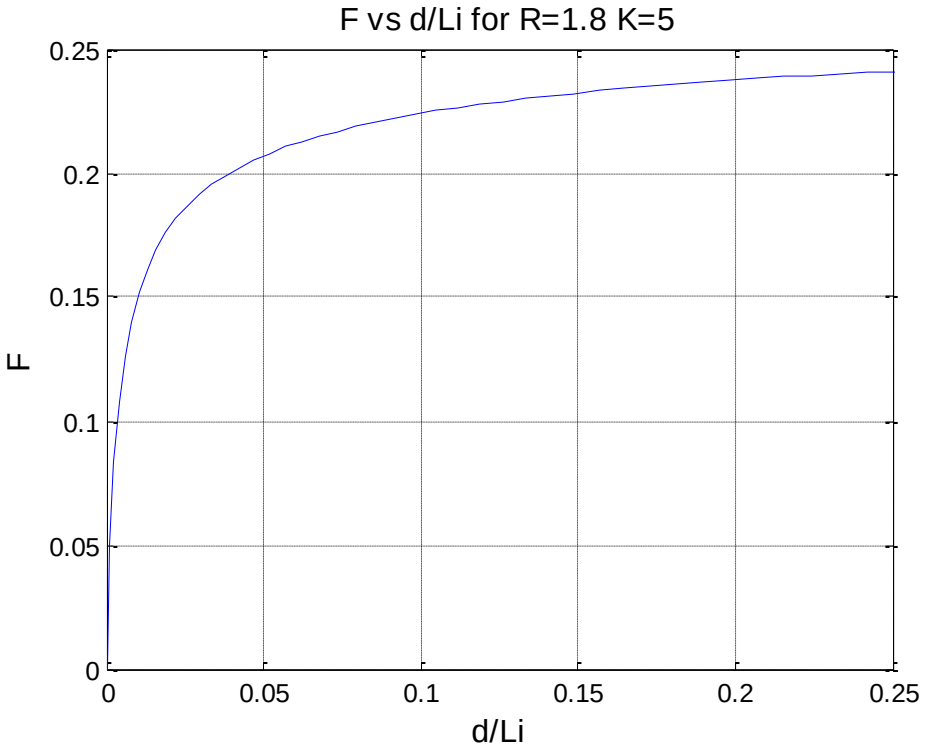

Figure 4.18 F vs d/L_i for data set 1 with θ_i=0.05, off-set -20 mm

4.1.4. Case 2

By following the same procedure as in Case 1, with the help of mathematical software, data set Case 2 is obtained. To observe the theoretical limit, θ_i is taken as 0 degree.

Parameter	Value	Unit
l_2	100	mm
l_3	150	mm
K	3.7	
θ_i	0	degree
β_i	0	degree
h	5	mm
w	1	mm

Table 4.6 Parameters of data set-2

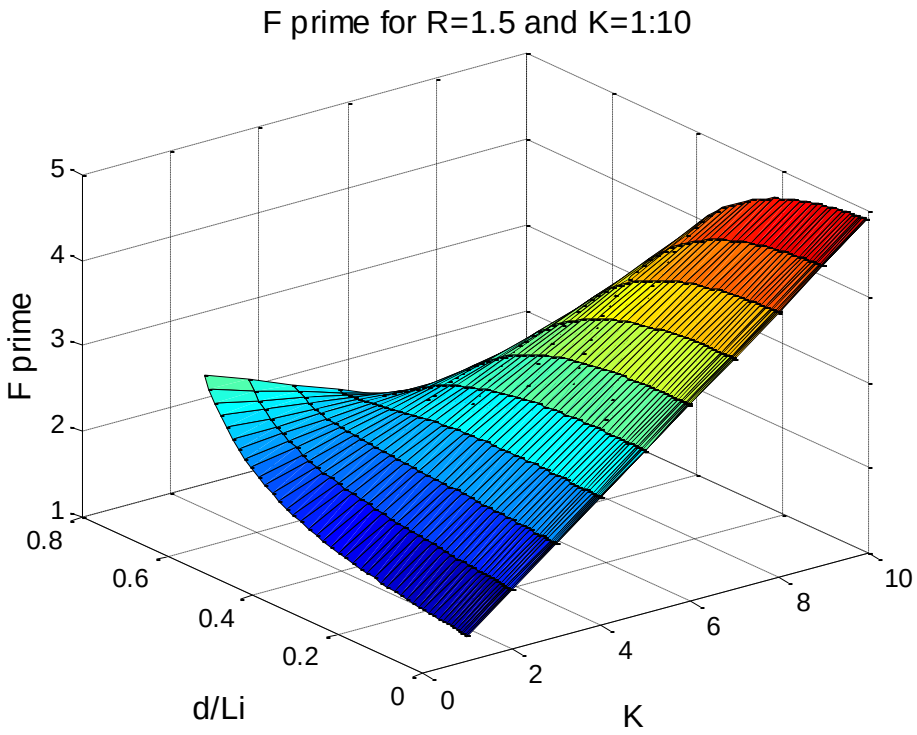

Figure 4.19 3D design chart of data set-2

As seen in Figure 4.19, at around K=3.7 there is a constant force region.

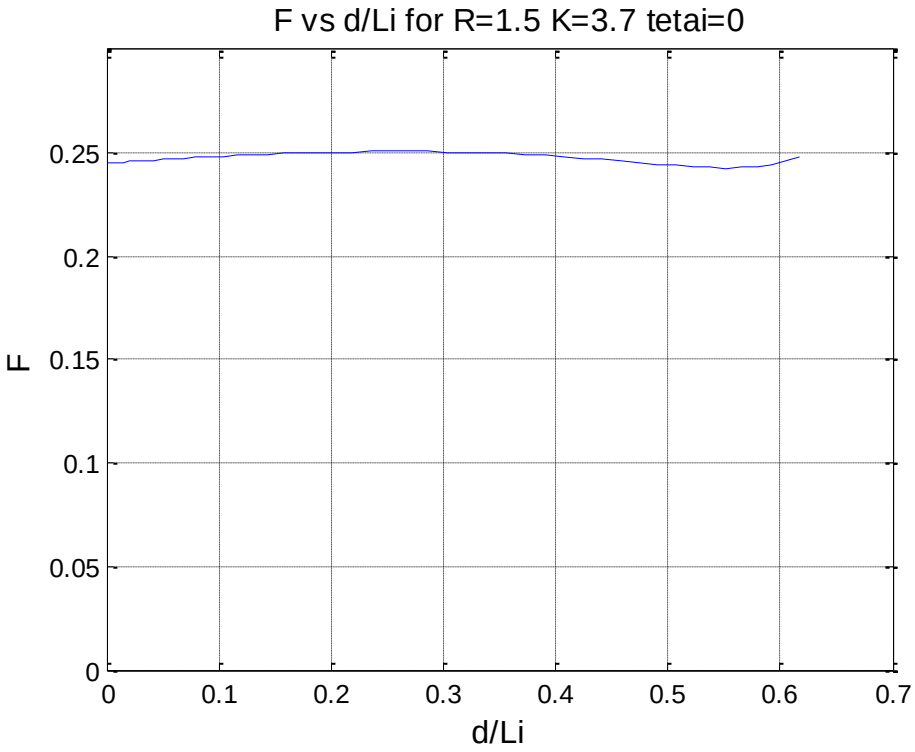

Figure 4.20 2D plot F vs d/Li of data set 2

As observed in Figure 4.20, there is a large constant force region at which the stroke is equal to 0.6168 with Ψ= 3.28 %.

However at the final position angle θ of link 2 is 100° which is very high. If θ is very high, there is a high non-linear deflection which may result very high stresses. Also for high values of θ, PRBM approach may become inconvenient according to the parameterization limits. Thus, at the verification part with FEM, θ is increased up to 58.5 degrees which corresponds to stroke=0.3 (Figure 4.21). In addition to these, θ_i is selected as 0.05 degrees to overcome inflection.

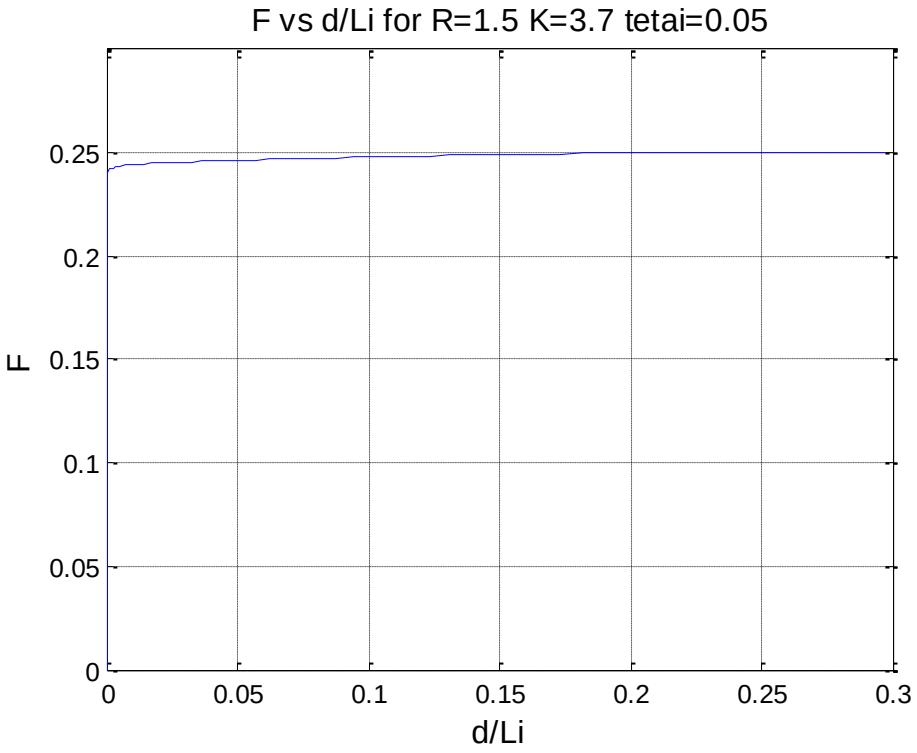

Figure 4.21 2D plot F vs d/Li of data set 2 θ_i =0.05

5. FEA ANALYSIS OF THE DESIGN MODEL

The constant force mechanism dimensions synthesized, constant force magnitudes and stress values calculated by parametric PRBM and virtual work method in the previous parts are now verified by a nonlinear finite element method. The flow chart below is going to be followed.

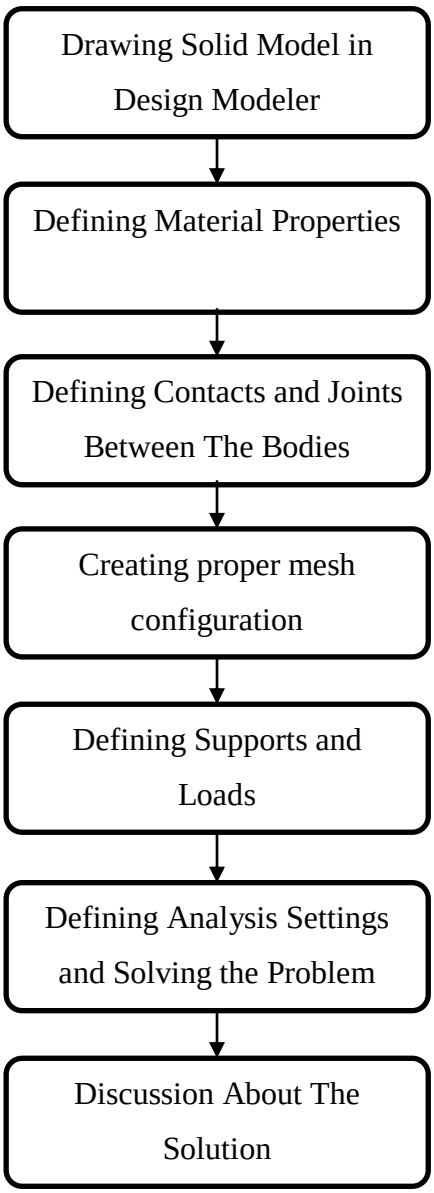

Figure 5.1 FEA Analysis Flow Chart

5.1. General Procedure of FEA with a Design Example

5.1.1. Analysis Type

Static Structural module is used in the analysis which is generally adequate and proper for compliant mechanism analysis due to relatively light mass of the links and assumed slow operation speed.

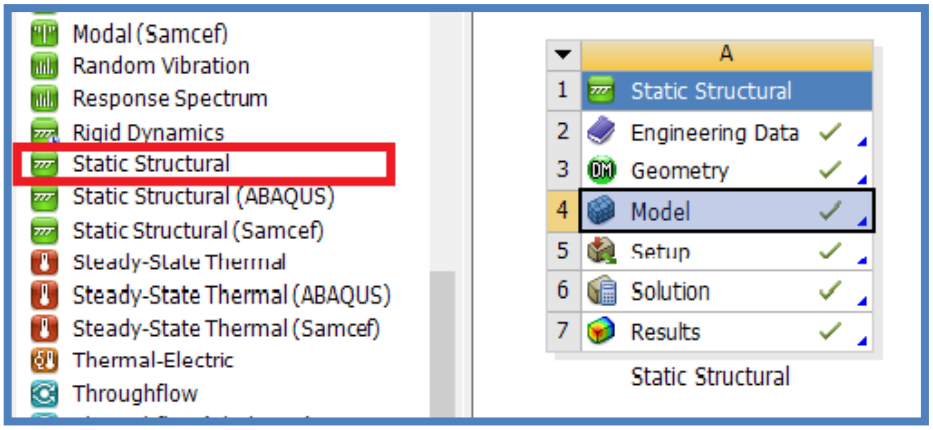

Figure 5.2 FEM Analysis Type

5.1.2. Material Definitions

Polypropylene has the following properties; E=1400 MPa and Poisson's ratio v=0.42

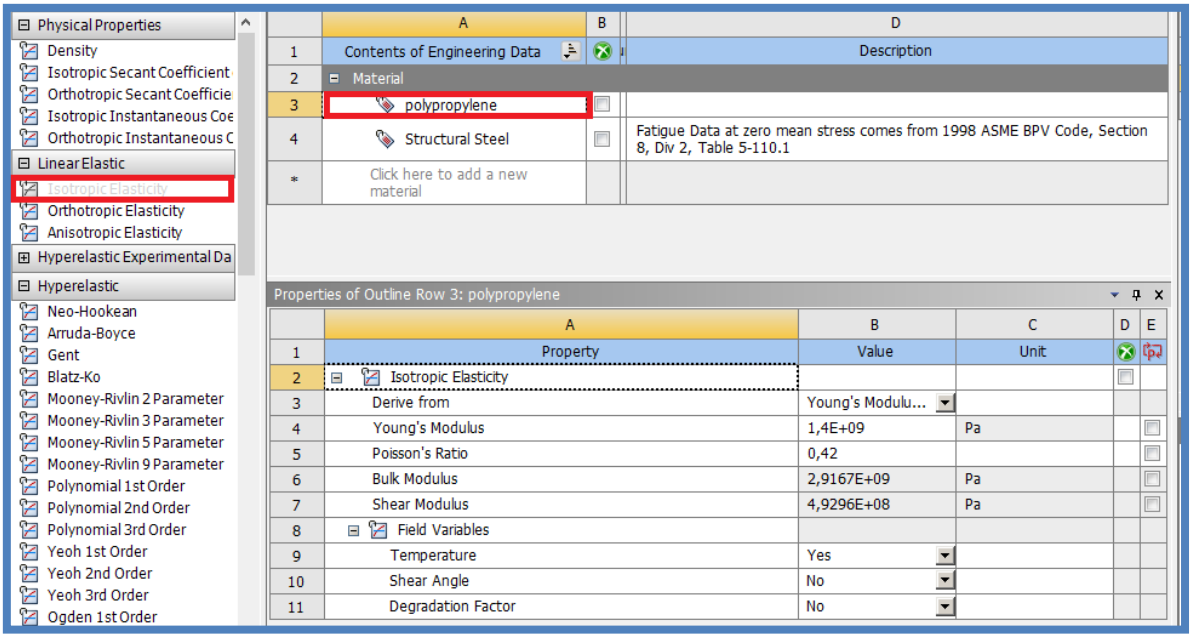

Figure 5.3 Polypropylene Material Properties

5.1.3. Drawing the Model in Design Modeler

Here, the dimensions and geometry of the model and pin joint's location are introduced. Also for detailed meshing, high stress locations are divided into separate parts. Fillets are added in order to avoid stress concentration.

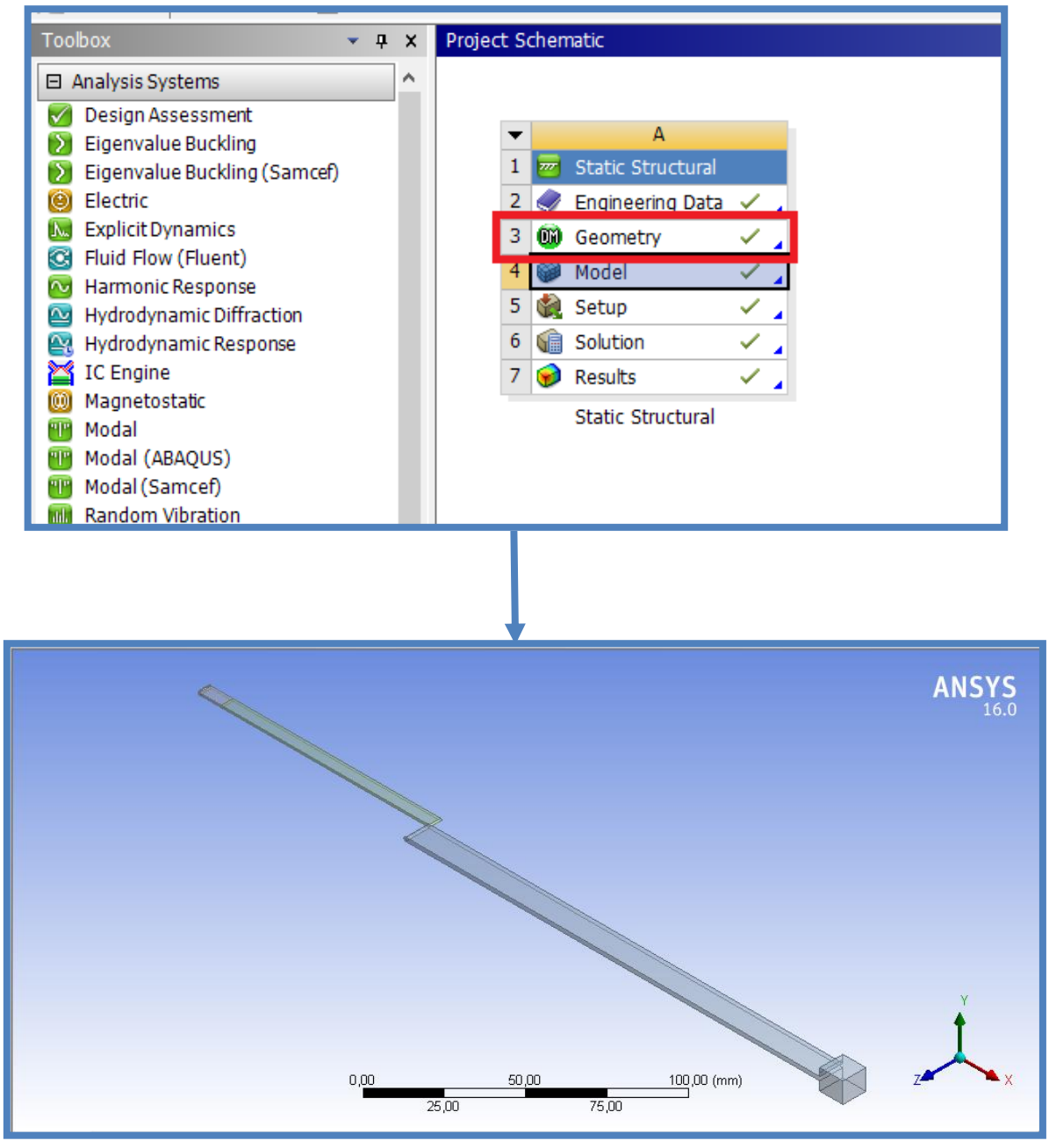

Figure 5.4 Design Model Drawing In Design Modeler

5.1.4. Model Settings

The analysis settings, part stiffness behavior and material assignments, joint definitions, general solver control settings, support and load definitions, stress solutions and probes are introduced step by step.

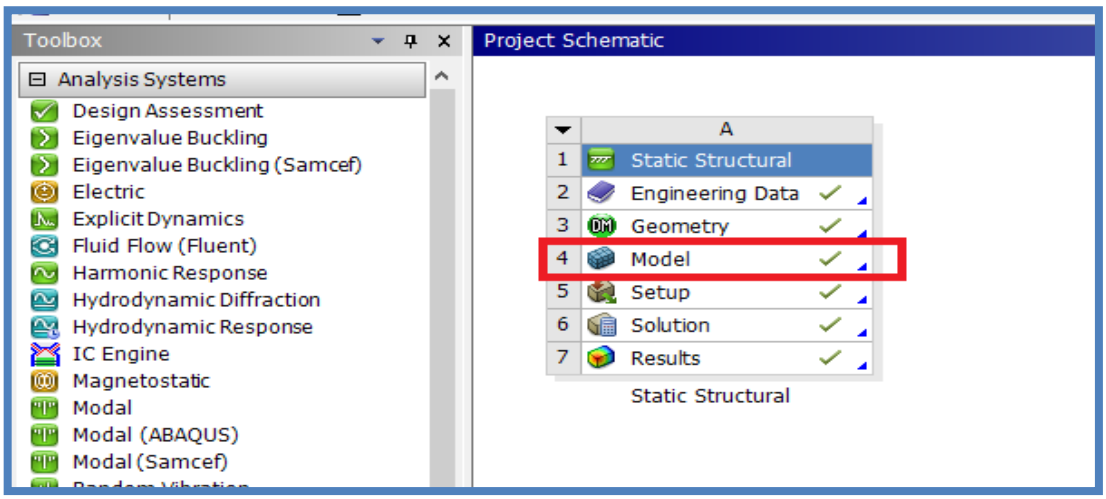

Figure 5.5 Entrance into Model Module

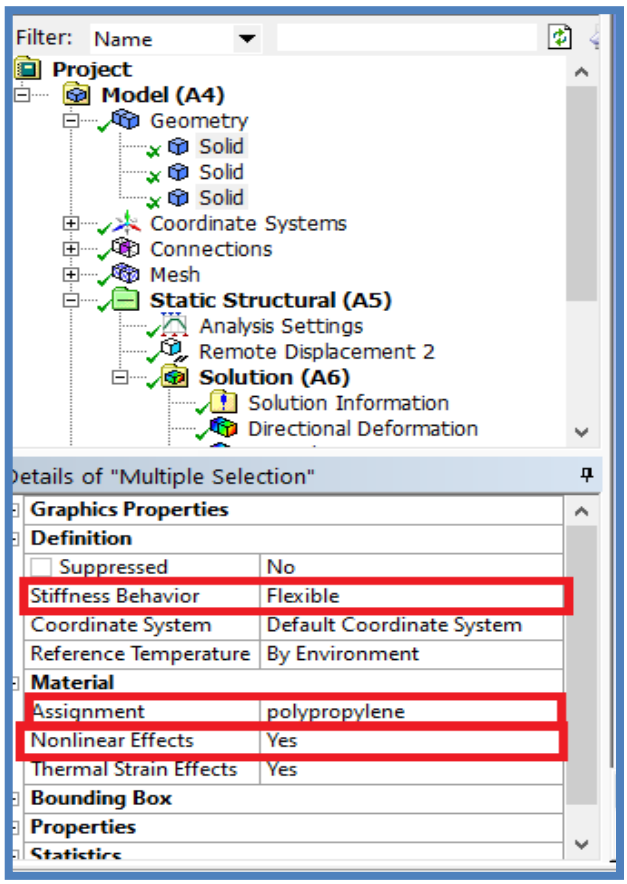

Figure 5.6 Part Stiffness Behaviour and Material Assignments

Fixed support is given from the left part of the link-2.

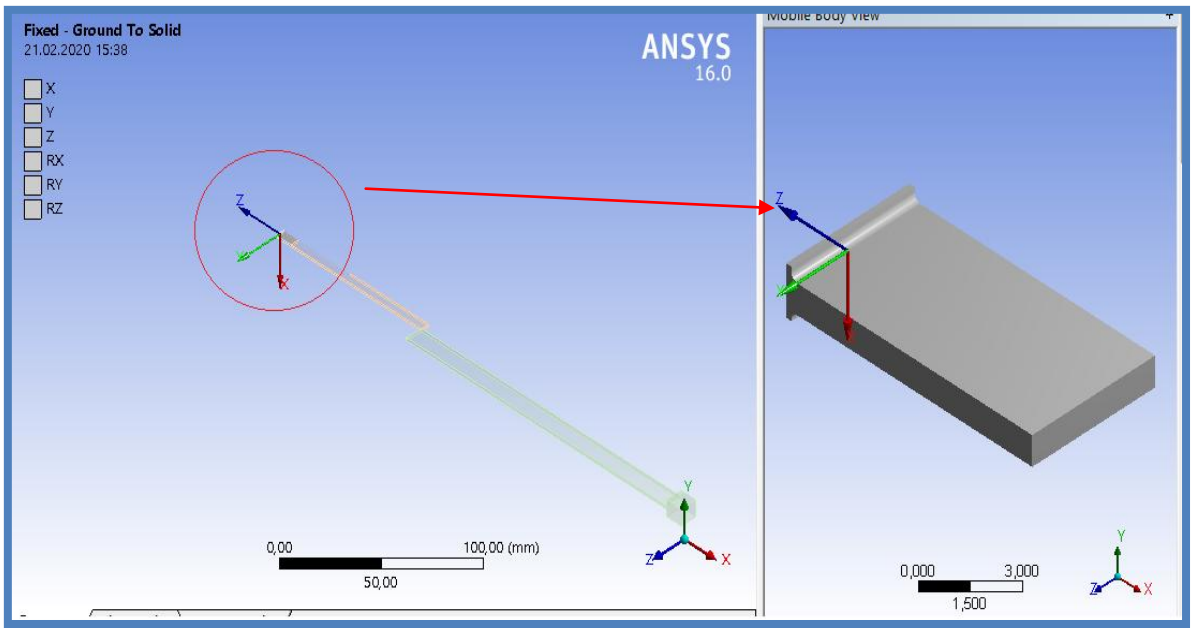

Figure 5.7 Fixed Support

Revolute joint is between the two links.

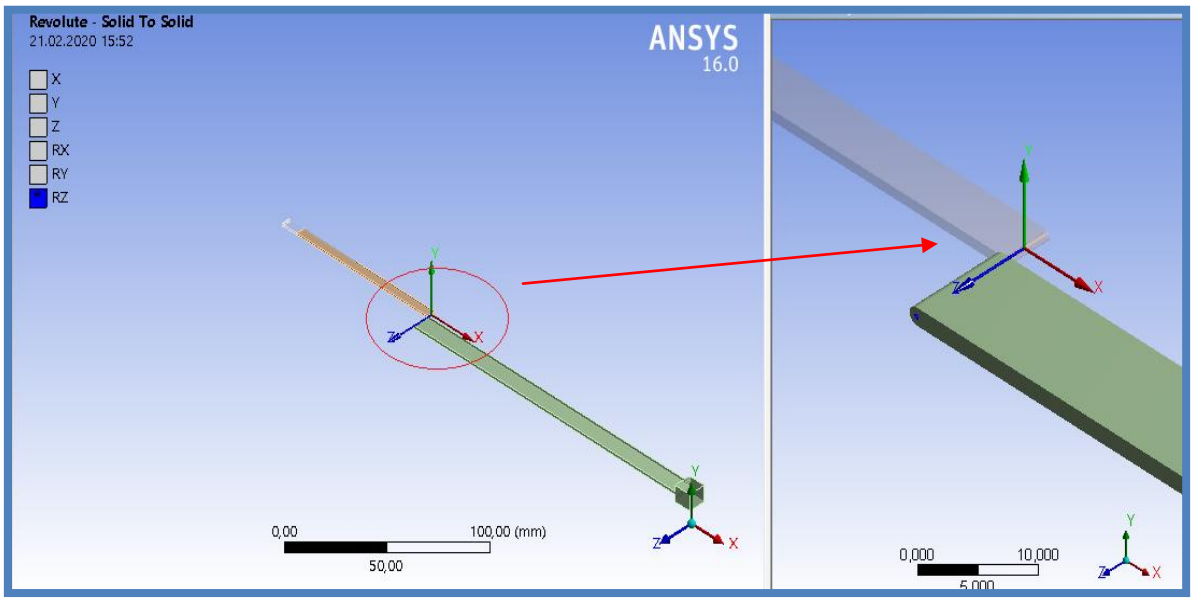

Figure 5.8 Revolute Joint

High stress is expected in the region close to the fixed support. So link-2 is separated into two parts in order to have detailed mesh in the high stress region. Bonded contact is defined between the two parts.

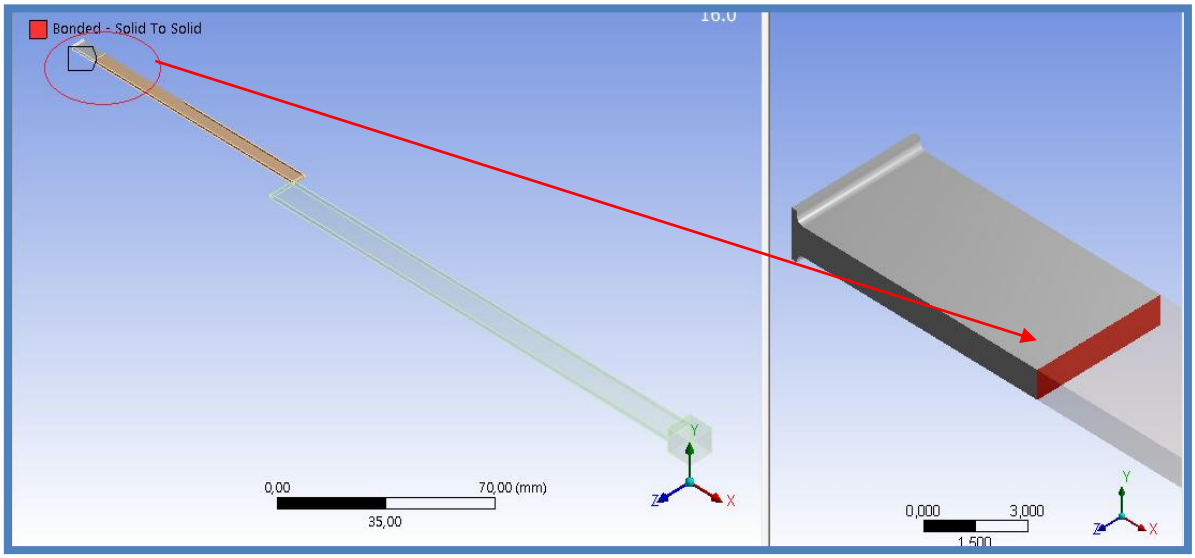

Figure 5.9 Bonded Contact

Mesh is generated using face sizing. Also to examine the critical regions smaller mesh size is constituted.

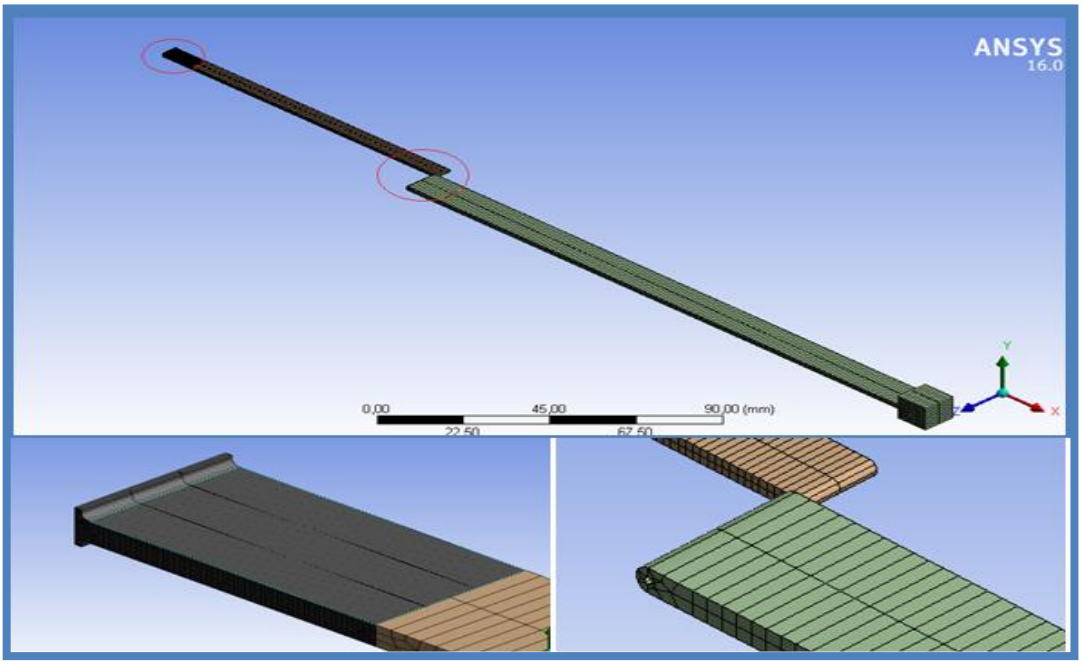

Figure 5.10 Mesh of the Model

60 mm of remote displacement is given to the slider in the –x direction which corresponds to approximately 58.5 ° of counter clockwise crank rotation and also 0.25 stroke to initial PRBM length according to the PRBM dimensions.

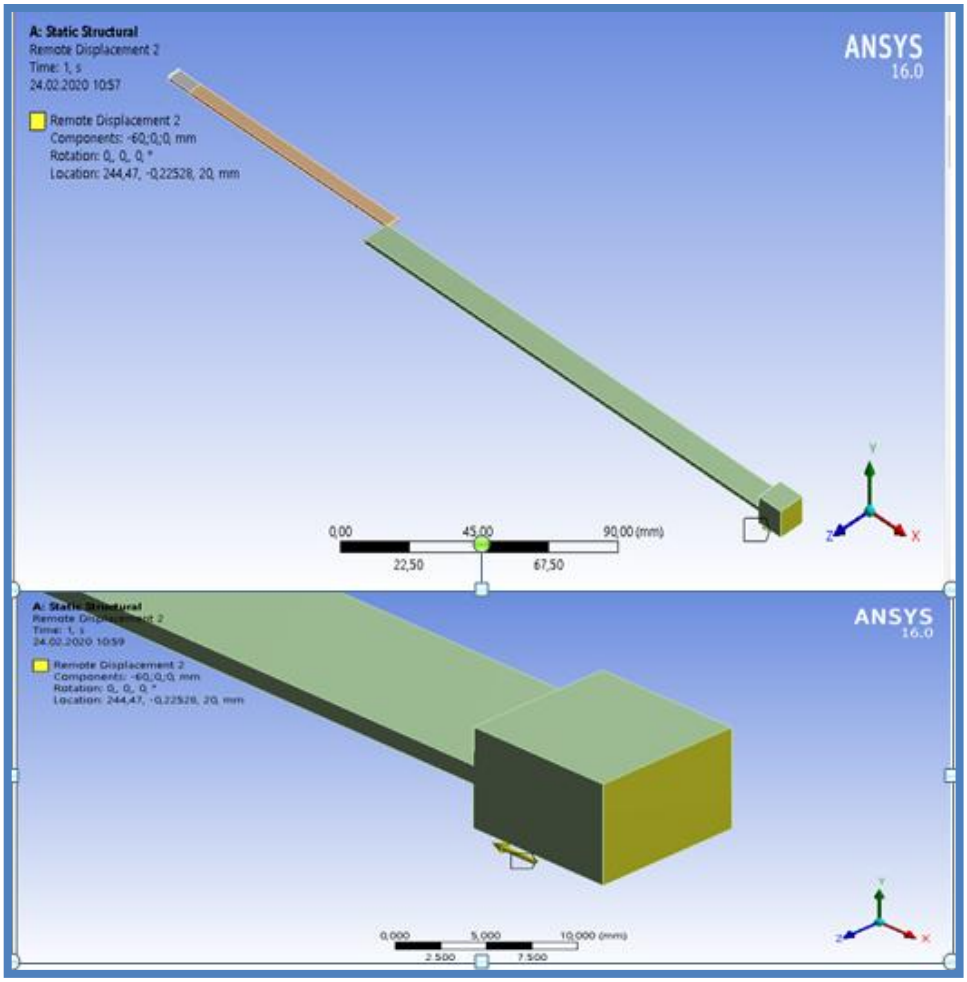

Figure 5.11 Remote Displacement

Analysis settings should be defined with time steps in order to overcome the convergence problems. Also large deflection must be on due to the large geometrical nonlinearities. As expected the motion of the model is largely based on the deflection of links, if proper values of time steps is not set, convergence issues encountered.

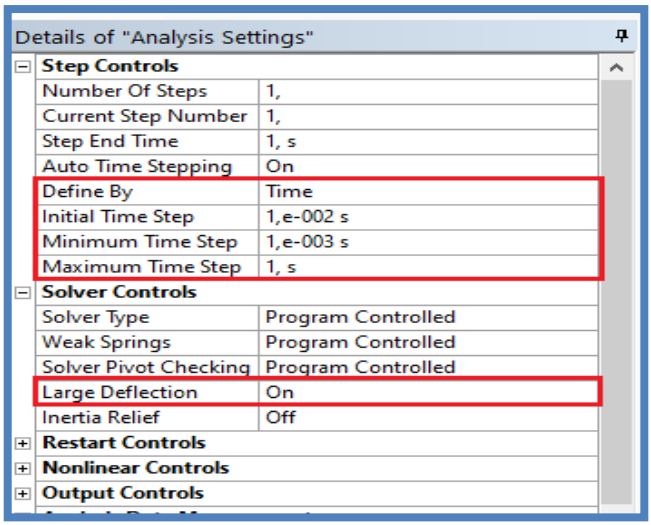

Figure 5.12 Analysis Settings

5.1.5. Solution Case 1

Maximum equivalent stress and normal stress values, reaction force at the output of the slider are studied. The force convergence graph is below. The problem is solved after 115 iterations.

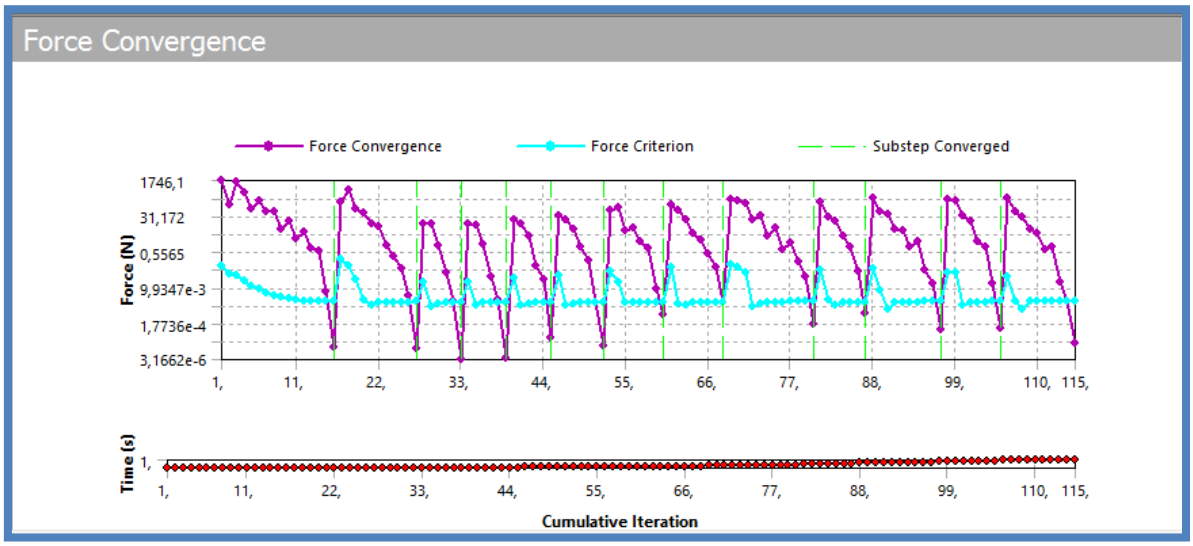

Figure 5.13 Force convergence graph

The maximum equivalent stress is 18.165 MPa (Figure 5.14) at the base of the fixed support of link-2.

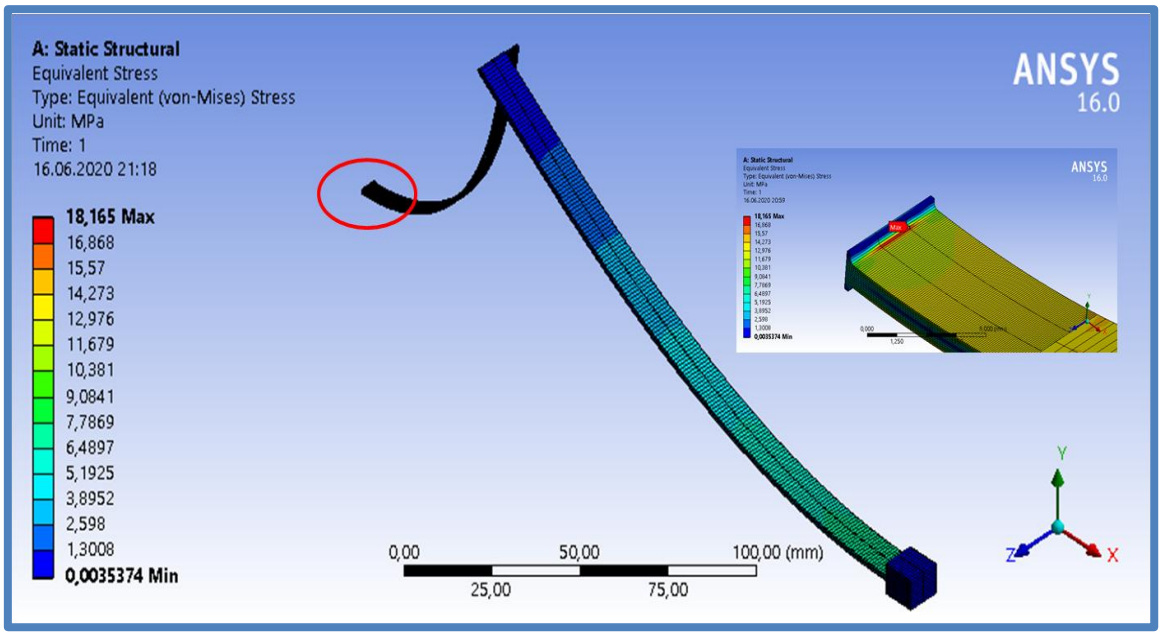

Figure 5.14 Equivalent Stress for Case-1

The normal stress is maximum at the base of Link-2 as expected (Figure 5.15). The value of the maximum normal stress is around 19.784 MPa at the top part of the cantilever beam. This value is close to the value of 21.9 MPa which is calculated as the result of our thesis theoretical approach even the PRBM is a rough approximation method generally done before nonlinear finite element analysis. Also using γ=0.85 and K_Θ=2.65 as average values causes some error.

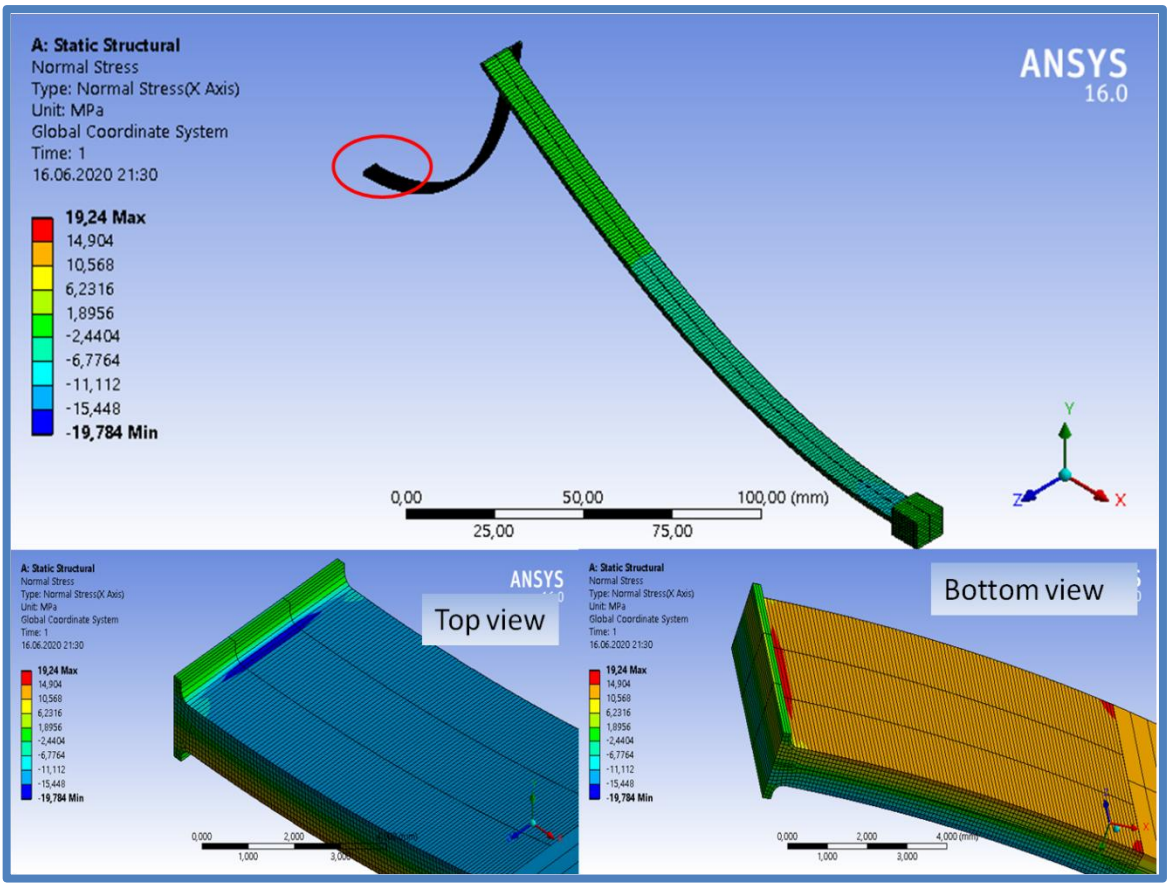

Figure 5.15 Normal Stress for Case 1

The reaction forces in the x direction calculated by the finite element software at the output of the mechanism is seen on Figure 5.16.

Tabular Data

	Steps	Time [s]	Directional Deformation (Min) [mm]	[B] Force Reaction (X) [N]
1	1	1,e-002	-0,61602	-0,23167
2	1	2,e-002	-1,2197	-0,23233
3	1	3,e-002	-1,8222	-0,23265
4	1	4,5e-002	-2,7249	-0,23295
5	1	6,75e-002	-4,0779	-0,23326
6	1	0,10125	-6,1062	-0,2336
7	1	0,15188	-9,1474	-0,23398
8	1	0,2025	-12,188	-0,2343
9	1	0,27844	-16,747	-0,2347
10	1	0,39234	-23,586	-0,23518
11	1	0,5632	-33,842	-0,23571
12	1	0,73406	-44,096	-0,23601
13	1	0,90492	-54,351	-0,2362
14	1	1,	-60,057	-0,23631

Figure 5.16 Reaction Forces Calculated By The FEA Software for Case 1

The average constant force reaction through the 60 mm displacement of the slider is 0.247 N with Ψ=%2.06 according to the parametric approach. There is close agreement with the FEA result average 0.234 N with Ψ = % 2.00. As mentioned in the discussions for the stress result, same reasons for error are valid. The PRBM is a rough approximation method and also using γ=0.85 and K_Θ=2.65 as average values for the whole displacement causes some error.

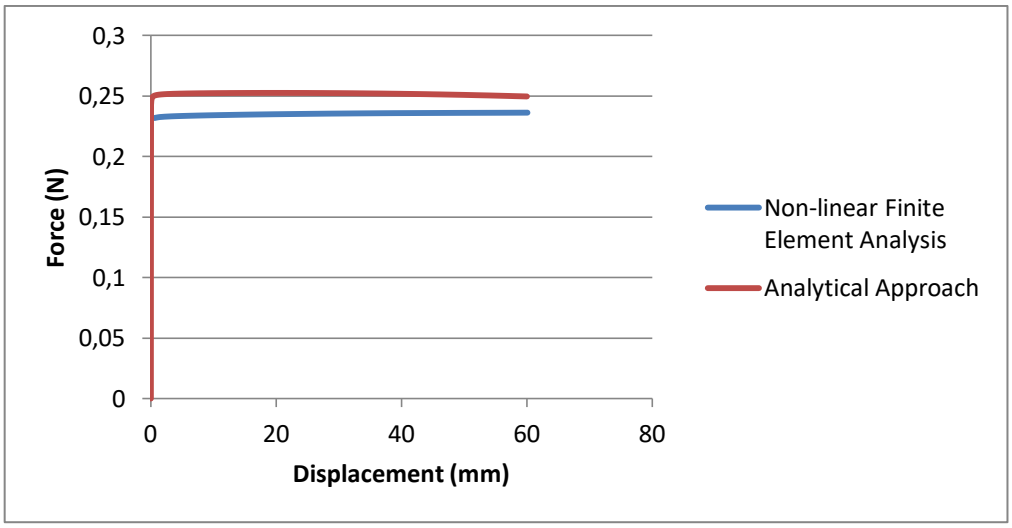

Figure 5.17 Case 1 reaction force comparision between fem and analytical approach

5.1.6. Solution Case 2

The force convergence graph is below. The problem is solved after 104 iterations.

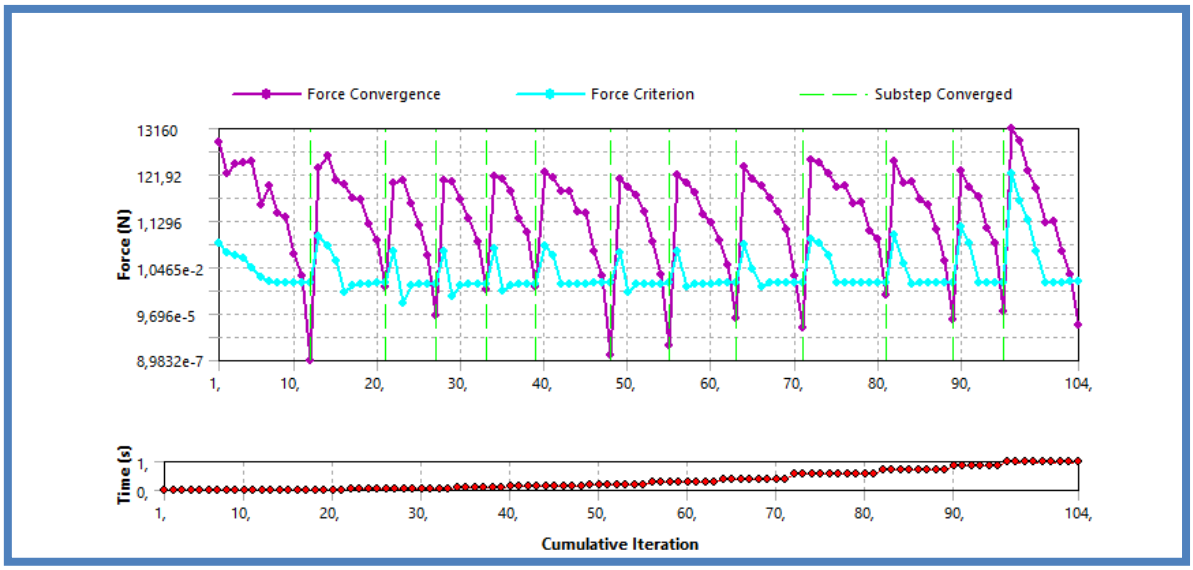

Figure 5.18 Case 2 Force convergence graph.

The maximum equivalent stress is 17.174 MPa at the base of the fixed support of link-2 (Figure 5.19).

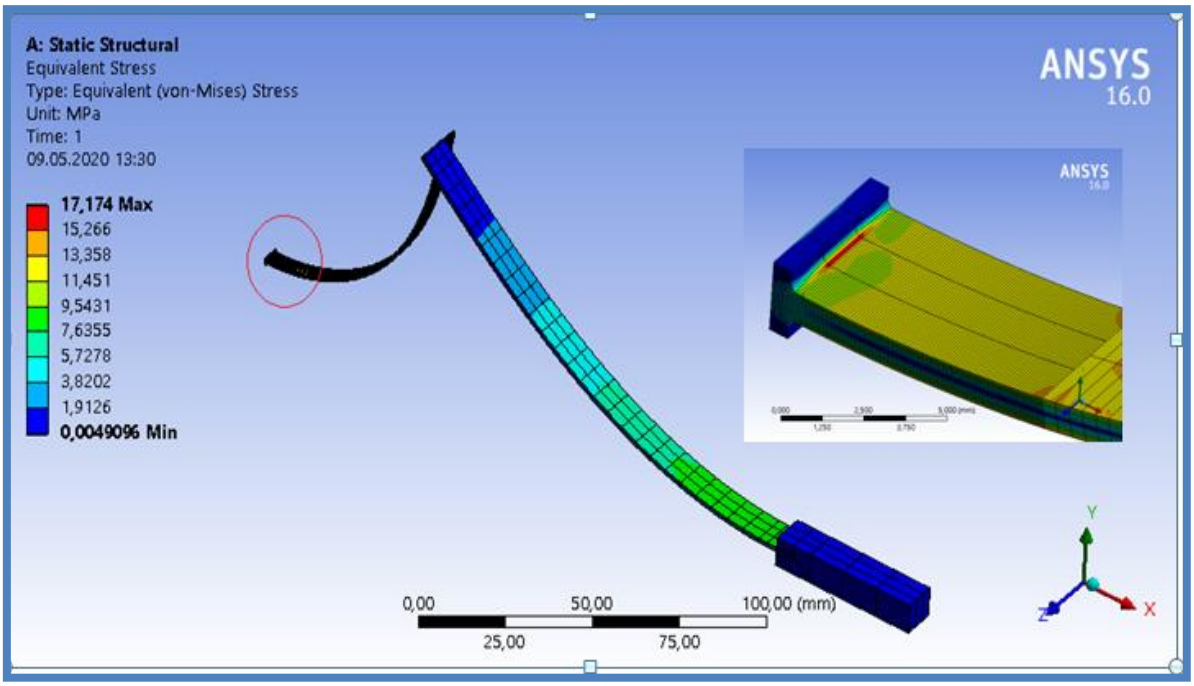

Figure 5.19 Case 2 Equivalent Stress

The normal stress is maximum at the base of link-2 as expected (Figure 5.20). The value of the maximum normal stress is around 18.236 MPa at the top of the cantilever beam. This value is close to the value of 21.5 MPa which is calculated as the result of our thesis theoretical approach. PRBM is a rough approximation method generally done before non linear finite element analysis. Also using γ=0.85 and K_Θ=2.65 as average values causes some error.

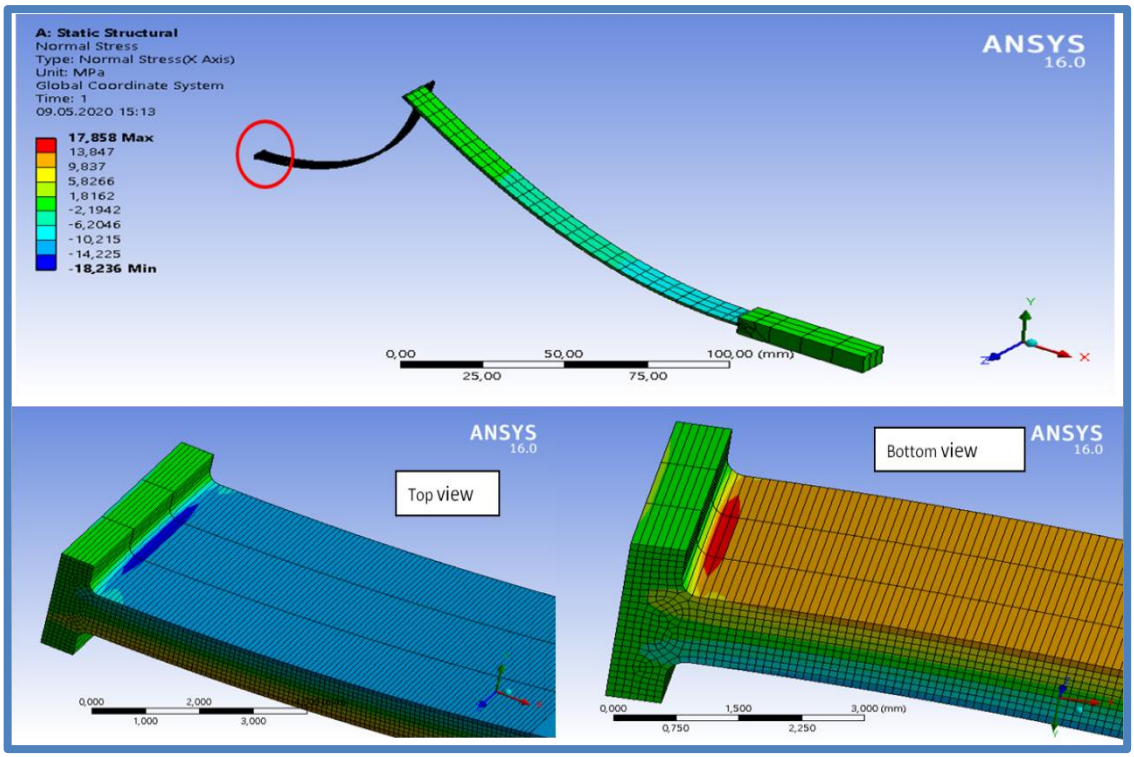

Figure 5.20 Case 2 Normal Stress

The reaction forces in the x direction calculated by the FEA software at the output of the mechanism is seen on Table 5.1.

Tabular Data

	Steps	Time [s]	Directional Deformation (Min) [mm]	[B] Force Reaction (X) [N]
1	1	1,e-002	-0,64835	-0,25326
2	1	2,e-002	-1,2842	-0,25405
3	1	3,5e-002	-2,2359	-0,25462
4	1	5,75e-002	-3,6615	-0,25515
5	1	9,125e-002	-5,7983	-0,25571
6	1	0,14188	-9,002	-0,25637
7	1	0,1925	-12,204	-0,25692
8	1	0,26844	-17,008	-0,25763
9	1	0,38234	-24,209	-0,25844
10	1	0,5532	-35,017	-0,25921
11	1	0,72406	-45,81	-0,25908
12	1	0,86203	-54,546	-0,2586
13	1	1,	-63,234	-0,25679

Table 5.1 Case 2 Reaction Forces Calculated By The Finite Element Software

The average constant force reaction through the 63.2 mm displacement of the slider is 0.247 N with Ψ=3.56 % according to the parametric approach. There is close agreement with the FEA result average 0.257 N with $\Psi = 2.3\%$. As mentioned in the discussions for the stress result, same reasons for error are valid. The PRBM is a rough approximation

method and also using γ=0.85 and K_{Θ}=2.65 as average values for the whole displacement causes some error.

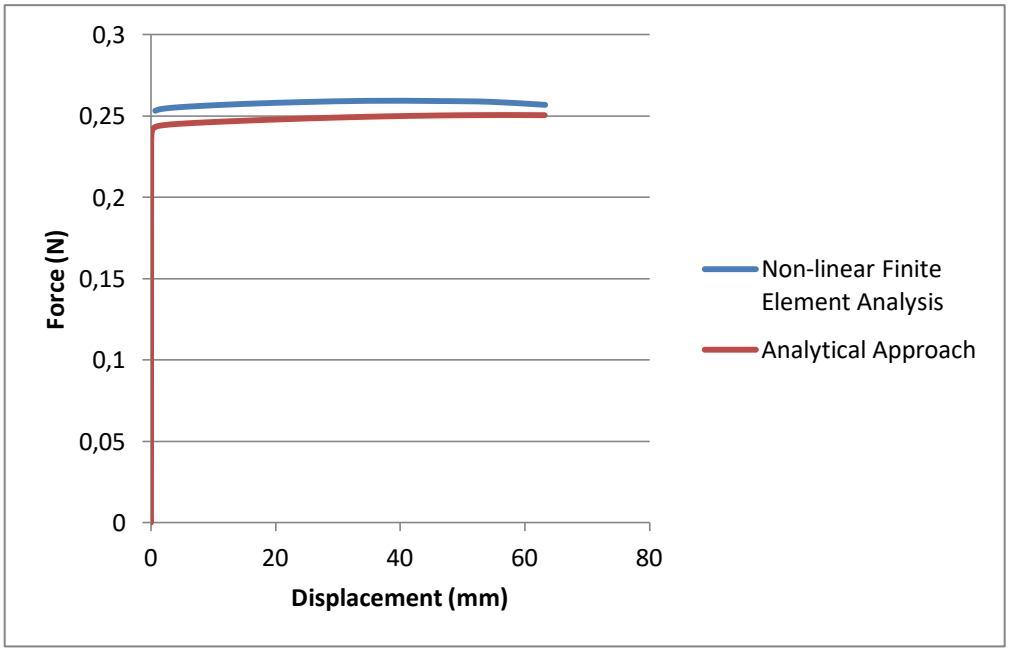

Figure 5.21 Case 2 Reaction Force Comparision between FEM and Analytical Approach

6. CONCLUSION

Compliant constant force mechanisms are popular in recent years. By using compliant members, constant force may be obtained by only mechanical means. Traditionally, constant force can be obtained by sensors and complex algorithms which make them expensive and unreliable.

Generally, a mechanism cannot have constant force properties from the initial deflection of the input. Thus, a transition zone is essential to reach the required force magnitude. However, due to the nature of mechanisms, a perfect constant force region cannot be obtained thus there is always some force fluctuation. The aim in designing constant force mechanism is to minimize the force fluctuation while maximizing the stroke.

In the thesis work, a slider crank based mechanism with two long flexible members with a revolute joint in the middle connection is proposed. The aim of the study is to determine dimension of the novel constant force mechanism which have maximum stroke with minimum force fluctuation.

First, general equation for the model is obtained by using PRBM and virtual work method together. This equation is converted into a dimensionless form which is more practical for interpreting the results independent from the dimensions. Then, 3D design charts are introduced for the optimization work to find the optimum dimension ratios and spring constant ratios with the maximum constant force characteristics. Generating 3D design charts eases to visualize and determine roughly where the maximum constant force range and minimum force magnitude variation exists. After deciding the constant force region by 3D optimization, detailed 2D inspection is done to find the exact values.

Moreover the effect of θ_i (the angle between the fixed link and horizontal line) is studied. θ_i is changed for the values between $0°$ and $10°$. It is observed that when the initial angle of the link with the horizontal increases, the constant force quality drops.

Also, to observe the effect of the off-set parameter, 10 mm and 20mm eccentricity is given in both negative and positive y directions to the mechanism. As a result, the eccentricity in both directions lessens the constant force characteristics.

Finally, two optimum data sets including link length and stiffness ratios are obtained as a result of the optimization work. The resultant stiffness ratios can be acquired by setting the width and height of the beams according to the moment of inertias of the beams. Both of these data sets are modeled with a FEA software. The result of the analytical parametric approach and finite element method turn out to be in a close agreement. We believe that, the large stroke constant force compliant mechanism proposed will be beneficial for applications requiring constant force. Also the 3D optimization procedure handled in this work will help the researchers working on constant force.

APPENDIX

THE DESIGN CODE

```
clc,clear all,close all hidden
format short
th2i=0; %%%%%%%%%%%%%%%%%%%%%%%%%%%%%%%%%%%%%%%%%%  change
teta2 initial
th2=linspace(th2i,58.5,50)
l2=100;%mm
l3=150;
gama=0.85
k_teta=2.65
r2=l2*gama;
r3=l3*gama;%mm  %%%%%%%%%%%%%%%%%%%%%%%%%%%%%%%  change l3/l2
R=r3/r2;  %  l3/l2,

c=0;  %%%%%%%%%%%%%%%%%%%%%%%%%%%%%%%%%%%%%%%%%%% change
offset

th3=(asind((c-r2*sind(th2))/r3)); % theta 3 coupler
beta=-th3
betai= beta(1); %beta initial

Linitial=r2*cosd(th2i)+r3*cosd(th3(1))  %total stroke,
initial length
Linstant=r2*(cosd(th2))+r3*(cosd(th3)) ; % instantaneous PRBM
length during motion
slider_travel=Linitial-Linstant        % distance travelled
by the slider
stroke_range=(Linitial-Linstant)/Linitial  %d/Li stroke range
K=3.7 ;%%%%%%%%%%%%%%%%%%%%%%%%%%%%%%%%%%%%%%%%  change k3/k2
for 2D plot

%virtual work method
alfa=cosd(th2)./cosd(beta);
w1=-R*((th2-th2i)/180*pi);
w2=-K*((beta-betai)/180*pi).*alfa;
w3=-w1-w2;
ds=(sind(th2)+tand(beta).*cosd(th2));
Fp=w3./ds; % F prime,


%to find F from F prime
w=5; %mm
h=1; %mm
I=w*h^3/12
E=1400 %Mpa for polypropylene
k2=gama*k_teta*E*I/l2  %change E wrt material type
F=Fp*k2/r3 %actual force N
```

```
%2D plot
figure(1),plot(stroke_range,F),
title('F vs d/Li for R=1.5 K=3.7','FontSize', 12)   %change
tetai wrt graph name
set(gca,'FontSize',10)
grid on;xlabel('d/Li','FontSize', 12);ylabel('F','FontSize',
12);

xlim([0 0.3])
ylim([0 0.3])

% To evaluate results

Fmax=max(F)
Fmin=min(F)
[m,n]=size(F); % m=1 n=size.

for i=1:1:n
    ratioFmax(i)=Fmax/F(i);
end

ratioFmax
sort_ratio=sort(ratioFmax)
ratio_limit=103.7; %%%%%%%%%%%%%%%%%%  change ratio
ratio_limit=ratio_limit/100
k=0;

for i=1:1:n
    if (ratioFmax(i)<ratio_limit)
     k=k+1;
     th2s(k)=th2(i);
     st(k)=slider_travel(i);
     sr(k)=stroke_range(i);
     F22(k)=F(i);
     Fint(k)=Fp(i);
    end
end
result=[th2s;sr;st;F22]

%Summary of the work

minteta_cons_zone=min(th2s)
maxteta_cons_zone=max(th2s)
total_cons_range=max(sr)-min(sr)
ratio_fmax_over_fmin=max(Fint)/min(Fint)
ratio_max_overall=max(sort_ratio(~isinf(sort_ratio)))
stroke_range_overall=max(stroke_range)
slider_travel_overall=max(slider_travel);
```

```
%stress calculations based on deflection
th2m=max(th2)/(180/pi);
P=k2*th2m/gama/l2/sin(1.57-th2m);
a=l2*(1-gama)+r2*cos(th2m);
b=r2*sin(th2m);
stress_MPa_n0=6*P*a/w/(h^2);

%reaction forces

T=k2.*th2/180*pi;
Fr2=F*r2.*sind(th2);
N=(T-Fr2)./r2./cosd(th2);


%3D  Plot

K=1:1:10;

for i=1:length(K)
    for j=1:length(th2)

    th3(j)=(asind((c-r2*sind(th2(j)))/r3)); % theta 3 coupler
    beta(j)=-th3(j);
    Linstant(j)=r2*(cosd(th2(j)))+r3*(cosd(th3(j))); % delta
x, calculating for range
    Y(i,j)=(Linitial-Linstant(j))/Linitial; %s/l
    alfa(j)=cosd(th2(j))./cosd(beta(j));
    w1(j)=-R*((th2(j)-th2i)/57.3);
    w2(i,j)=-K(i)*((beta(j)-beta(1))/57.3).*alfa(j);
    w3(i,j)=-w1(j)-w2(i,j);
    ds(j)=(sind(th2(j))+tand(beta(j)).*cosd(th2(j)));
    Z(i,j)=w3(i,j)./ds(j);
    X(i,j)=K(i);
    end
end

figure(2)
surf(X,Y,Z)
set(gca,'FontSize',10)
xlabel('K','FontSize', 12)
ylabel('d/Li','FontSize', 12)
%ylim([0 0.3])
zlabel('F prime','FontSize', 12)
title('F prime for R=1.8 and K=1:10 stroke=0.4','FontSize',
12)
```

REFERENCES

[1] G. N. Sandor and A. G. Erdman, *Advanced Mechanism Design V. 2: Analysis and Synthesis*. Prentice-Hall, 1984.

[2] L. L. Howell, *Compliant mechanisms*. John Wiley & Sons, 2001.

[3] E. Tanık, "Transmission angle in compliant slider-crank mechanism," *Mechanism and Machine Theory* vol. 46, no. 11, pp. 1623-1632, 2011.

[4] P. Wang and Q. Xu, "Design and modeling of constant-force mechanisms: A survey," *Mechanism and Machine Theory,* vol. 119, pp. 1-21, 2018.

[5] L. L. Howell and A. Midha, "A method for the design of compliant mechanisms with small-length flexural pivots," *Journal of mechanical design,* vol. 116, no. 1, pp. 280-290, 1994.

[6] J. E. Shigley, *Shigley's mechanical engineering design*. Tata McGraw-Hill Education, 2011.

[7] R. N. Motsinger, "Flexural devices in measurement systems," *Measurement Engineering,* vol. 1, pp. 383-435, 1964.

[8] D. R. Nahar and T. Sugar, "Compliant constant-force mechanism with a variable output for micro/macro applications," in *2003 IEEE International Conference on Robotics and Automation (Cat. No. 03CH37422)*, 2003, vol. 1, pp. 318-323: IEEE.

[9] R. Nathan, "A constant force generation mechanism," *Journal of Mechanisms, Transmissions, Autpmation in Design,* vol. 107, no. 4, pp. 508-512, 1985.

[10] A. Carrella, M. Brennan, T. J. J. o. M. S. Waters, and Technology, "Optimization of a quasi-zero-stiffness isolator," vol. 21, no. 6, p. 946, 2007.

[11] Y. Liu, D.-J. Li, D.-p. Yu, J.-g. Miao, J. J. M. B. D. o. S. Yao, and Machines, "Design of a curved surface constant force mechanism," vol. 45, no. 2, pp. 160-172, 2017.

[12] U. Rahman and H. Zhou, "Design of constant force compliant mechanisms," *Int. J. Eng. Res. Tech.,* vol. 3, no. 7, pp. 14-19, 2014.

[13] C.-C. Lan, J.-H. Wang, and Y.-H. Chen, "A compliant constant-force mechanism for adaptive robot end-effector operations," in *2010 IEEE International Conference on Robotics and Automation*, 2010, pp. 2131-2136: IEEE.

[14] L. L. Howell, A. Midha, and M. Murphy, "Dimensional synthesis of compliant constant-force slider mechanisms," 1994.

[15] E. R. Johnston, F. Beer, and E. Eisenberg, *Vector Mechanics for Engineers: Statics and Dynamics*. McGraw-Hill, 2009.